



This is to certify that the

dissertation entitled

## **DOLOMITE KINETICS**

presented by

## Stephan Harold Nordeng

has been accepted towards fulfillment of the requirements for

degree in

Ph.D.

Geology

Date March 11, 1914

MSU is an Affirmative Action/Equal Opportunity Institution

0-12771

## LIBRARY Michigan State University

PLACE IN RETURN BOX to remove this checkout from your record. TO AVOID FINES return on or before date due.

DATE DUE	DATE DUE	DATE DUE
MAGIC 2		
JAN 2 4 1999		
OCA \$2970 300		

MSU is An Affirmative Action/Equal Opportunity institution cycles/datedus.pm3-p.1

July a.

10

\***}\***@\*(\$0)

## **DOLOMITE KINETICS**

By

**Stephan Harold Nordeng** 

## **A DISSERTATION**

Submitted to

Michigan State University

in partial fulfillment of the requirements

for the degree of

**DOCTOR OF PHILOSOPHY** 

**Department of Geological Sciences** 

1994

### Abstract

#### DOLOMITE KINETICS

by

#### STEPHAN HAROLD NORDENG

Factors governing nucleation in the transition of calcite to dolomite at 1930 C in 1 M, 0.66 Mg to Ca ratio solutions were investigated. Nucleation and crystal growth kinetics were determined from differences in the induction period between isothermal experiments and experiments cycled between 1930 C and room temperature. The cycled reactions used 12 hour and 48 hour heating periods interchanged with 12 hours at room temperature. All three experimental designs produced high magnesium calcite (HMC), nonstoichiometric dolomite and near ideal dolomite. These experiments show that HMC nucleates in less than 12 hours but dolomite nucleation requires between 12 and 48 hours of heating. Surface reaction, diffusion, and reactant supply rates may limit crystal growth rates. These limits may be determined from normalized measurements of cathodoluminescent zoned (CL) crystals. Zone thickness data were obtained from samples of dolomite taken from the Burlington-Keokuk (Miss.), Saluda (Ord.), Ft. Payne (Miss.) and Seroe Domi (Plio.) Formations. All of the samples exhibited a linear relationship between the crystal radius and zone

thickness. This zonation pattern may be explained in several ways. Assuming continuous nucleation, spatial solution homogeneity and constant reaction rate coefficient, these data may reflect growth consistent with a 2-D nucleation and layer growth model. These data may also reflect a size-dependent growth rate. The data are also consistent with almost any crystal growth model in which nucleation is assumed to be instantaneous, but small scale inhomogeneities exist in solution composition. Such inhomogeneity may be caused by depletion of solute by reactions during aqueous transport.

### **ACKNOWLEDGEMENTS**

I would like to thank the members of my committee,
Dr. Duncan Sibley, Dr. Michael Velbel, Dr. David Long and
Dr. Grahame Larson for their guidance in completing this
dissertation. I would especially like to thank Dr.
Sibley for his patience and remarkable insight into the
significance of aspects of this study that would have
otherwise eluded me.

I would like to thank Drs. William Last, Sal

Mazzullo and one anonymous reviewer for their

constructive criticisms of an early version of Part 1 of

this manuscript. I would also like to thank Dr. William

Carlson for his insightful review of an early version of

Part 2. I am grateful to the Donors of The Petroleum

Research Fund, administered by the American Chemical

Society for their financial support.

Finally, I thank my wife Betty for her stability and love throughout this experience.

## TABLE OF CONTENTS

List	of Figures	Vi
List	of Tables	vii
PART	I Dolomite Stoichiometry and Ostwalds Step Rule	
	Abstract	
	Introduction	1
	Ostwald' Step Rule and Nucleation Kinetics	3
	Nucleation Under Oscillating Temprature	6
	Experimental Procedure	10
	Results	13
	Discussion	23
	Conclusions	28
	Bibliography Part I	32
Part	II Constraints on the Rate-Limiting Step Governi Dolomite Crystal Growth	ng
	Abstract	33
	Introduction	35
	Crystal Growth	39
	Surface-Reaction-Limited Growth	40
	2-D Nucleation-Monolayer Growth	41
	Mononuclear Layer Growth	42
	Polynuclear Growth	43
	Screw Dislocation Limited Growth	44
	Diffusion Limited Growth	44
	Diffusion Limited Growth  Methods	44 48

Sample Characterization	56
Seroe Domi	56
Burlington-Keokuk	57
Ft. Payne	59
Saluda Formation	60
Results	62
Discussion	69
Growth of Homogeneous Crystal from Homogeneous Solutions	69
Size Dependent Growth from Homogeneous Solution	69
Crystal Growth from Compositionally Inhomogeneous Solutions	70
Conclusions	82
Bibliography Part II	84
APPENDICES	88
COMBINED BIBLIOGRAPHY	119
List of Tables	
PART I Table 1 Experimental results	16
PART II Table 1 Summary of Growth Laws	47
APPENDIX I Reaction Data for Part I	88
APPENDIX II Table A2.1 Crystal measurements.for PART II	101
APPENDIX III Table A3 data used in Fig. 5 of	118

## List of Figures

## PART I

Figure		
1	Generalized thermodynamic stability diagram of hemisherical ion clusters on a planar substrate	9
2	Results of the 48 hour cycled experiments and the isothermal baseline	20
3	Results of the 12 hour cycled experiments and the isothermal baseline	22
4	Generalized results of dolomitization experiments	26
	PART II	
Figure		
1	Schematic diagram of a CL zoned crystal with measured parameters	51
2	Triangle constructed from measurements in Fig. 1	51
3	Type curves for the normalized growth laws considered in PART II	55
4	Normalized radius-rate data plotted on type curves.	
	a) Burlington-Keokuk Fm., Biggsville Quarry	64
	b) Burlington-Keokuk Fm., Harper Quarry	65
	c) Seroe Domi Fm., Bonaire	66
	d) Ft. Payne Fm., Jellico, Tenn	67
	e) Saluda Fm., Madison, Ind	68
5	Observed Mg <sup>2+</sup> gradients plotted with theoretic gradients due to various reaction rates	79

# List of Figures (cont.)

<b>A</b> 1	DDI	7ND	TY	TT

A2.1	Schematic diagram of a CL zoned crystal with measured parameters	100
A2.2	Triangle constructed from measurements in Fig. A2.1	100

## PART I

## Introduction

Stoichiometric, ordered dolomite is very rare in modern sediments in spite of the fact that it is the thermodynamically most stable carbonate mineral in seawater. As a result, questions exist concerning the thermodynamic and kinetic factors that influence dolomitization (Machel and Mountjoy, 1986; Hardie, 1987). High temperature experiments (>100°C) provide insight into the general process of dolomitization (Goldsmith et al. 1961; Katz and Matthews, 1977; Gaines, 1980; Baker and Kastner, 1981; Sibley et al., 1987; Sibley, 1990). At high temperatures, stoichiometric and ordered dolomite forms through a series of dissolution-reprecipitation reactions involving an initial calcium carbonate reactant and a Mq-rich solution. Experimental dolomitization is sensitive to temperature, solution chemistry, reactant texture and reactant mineralogy. Like many reactions, experimental dolomitization rates increase with temperature (Katz and Matthews, 1977), and the degree of dolomite supersaturation as measured by reactant concentrations,  $Mg^{2+}/Ca^{2+}$  ratios, carbonate alkalinity and pCO2 (Gaines, 1980; Sibley et al. 1987). Traces of dissolved sulfate in chloride solutions containing Mg, Ca and Na supress dolomitization, either by suppressing nucleation or surface reaction rates, or by complexing ions and thereby modifying solution chemistry (Baker and Kastner, 1981). Experimentation also shows that

increasing the surface area of the reactant enhances reaction rates (Katz and Matthews, 1977; Gaines, 1980; Sibley et al., 1987). The mineralogy of the reactant also affects dolomitization rates (Katz and Matthews, 1977; Baker and Kastner, 1981; Sibley and Bartlett, 1987). Katz and Matthews, (1977) found that aragonite formed dolomite more rapidly than calcite and that calcite was dolomitized faster than Mg-calcite.

The importance of nucleation barriers to dolomitization has been tested using seeded experiments. Gaines (1980) found that experimentally produced "protodolomite" seeds decreased the time required to form dolomite. However, Sibley and Bartlett (1987) found that adding stoichiometric dolomite seeds failed to increase dolomitization rates. These results suggest that the composition of the seed is an important but poorly constrained variable in promoting dolomite nucleation.

A significant period of time precedes the appearance of the first reaction product in many dolomitization experiments (Katz and Matthews, 1977; Sibley and Bartlett, 1987). Walton (1969) referred to such intervals as the "induction period". Following the induction period, dolomitization reactions proceed rapidly, producing the metastable phases high-Mg calcite (HMC) and calcian dolomite before stoichiometric, ordered dolomite is formed (Katz and Matthews, 1977; Baker and Kastner, 1981; Sibley et al., 1987; Sibley, 1990). These observations are consistent with

Ostwald's Step Rule, in that less stable, intermediate phases form before the final, most stable product. In this paper, we present new experimental results which verify the hypothesis that Ostwald's Step Rule in dolomitization is determined by nucleation kinetics. We also show that significant nucleation occurs early in the reaction and that the length of the induction period is therefore due to slow initial growth of metastable phases.

## Ostwald's Step Rule and Nucleation Kinetics

Ostwald's Step Rule states that a reaction proceeds through a series of intermediate phases, each thermodynamically more stable than the preceding (Ostwald, 1897, in Casey and Morse, 1988). This progression through different phases is controlled by the rates of both nucleation and crystal growth of each phase (Dunning, 1969; Morse and Casey, 1988). Therefore, the kinetics either of nucleation or crystal growth may be responsible for producing the intermediate phases in the calcite-to-dolomite transformation. If this is so, then heterogeneous nucleation theory should provide a basis for testing the importance of nucleation in establishing the order in which intermediate phases appear (Nielsen, 1964, Berner; 1971; Steefel and Van Cappellen, 1990). Equation 1 describes heterogeneous nucleation as the sum of a bulk or thermodynamic energy term and a surface free energy term.

Under supersaturated conditions, the bulk free energy term drives the system towards precipitation whereas the surface free energy term drives the system towards dissolution. During heterogeneous nucleation, clusters of ions form on some substrate and are energetically unstable until they reach critical size. Critical size is achieved when the addition of ions produces a net free energy ( $\delta G[n]$ ) in Eq. 1 that is less than or equal to zero. The first term on the right hand side of Eq. 1 describes the bulk or cluster free energy as a function of the number of unit cells of the mineral in the cluster (n), Boltzman's constant  $(k_h)$ , temperature (T) and saturation state of the precipitating mineral relative to the solution  $(\Omega)$ .  $\delta G_{ex}$  is the free energy associated with the surface of the cluster. Therefore, stable nucleation is attained when the bulk free energy is greater than, or equal to, the surface free energy  $(\delta G[n] \leq 0)$  (Nielsen, 1964; Steefel and Van Cappellen, 1990).

Eq. 1 
$$\delta G[n] = -n k_b T \ln \Omega + \delta G_{ex}(n)$$

Where:

$$\Omega = IAP/K_{eq}$$

If a nucleus is a hemisphere with a radius r lying on a planar substrate then the minimum size it must attain before becoming stable ( $\delta G[n] = 0$ ) is given by the critical radius

(r\*) in Eq. 2 (Nielsen, 1964; Berner, 1971; Steefel and Van Cappellen, 1990):

Eq. 2 
$$r^* = v \sigma/(k_b T \ln \Omega)$$

Where v is the molar volume and  $\sigma$  is the surface free energy coefficient. The activation energy required to achieve a critical radius is defined by Eq. 3 as  $\delta G^*$  (Steefel and Van Cappellen, 1990):

Eq. 3 
$$\delta G^* = \pi v^2 \sigma^3 / 3 (k_b T \ln \Omega)^2$$

Steefel and Van Cappellen (1990) developed an expression for heterogeneous nucleation rates from Nielsen's (1964) classical description of homogeneous nucleation. In this treatment heterogeneous nucleation rates are assumed to increase exponentially as a function of the activation energy  $\delta G^{*}$ .

Eq. 4 
$$N^* = N \exp(-\delta G^*/k_bT)$$

where N<sup>±</sup> is equal to the surface density of critical nuclei, and N is the average density of mineral units in the adsorption layer surrounding the substrate. Equation 4 clearly shows that when N is constant, nucleation of the phase with the smaller activation energy is favored over phases with greater activation energies. Therefore, the

average stability of nuclei formed by competing phases may be used to evaluate the relative magnitude of each phase's activation energy ( $\delta G^{\pm}$ ).

Equation 3 shows that  $\delta G^*$  depends on v,  $\sigma$  and  $\Omega$ . If two phases have essentially constant  $v^2$  and  $\sigma^3$  relative to the difference in  $\ln (\Omega)$ ,  $\delta G^*$  favors nucleation of the least soluble phase (larger  $\Omega$ ). However, when the difference in  $v^2$  and/ or  $\sigma^3$  is dominant then  $\delta G^*$  favors nucleation of the phase with the smaller v or  $\sigma$ .

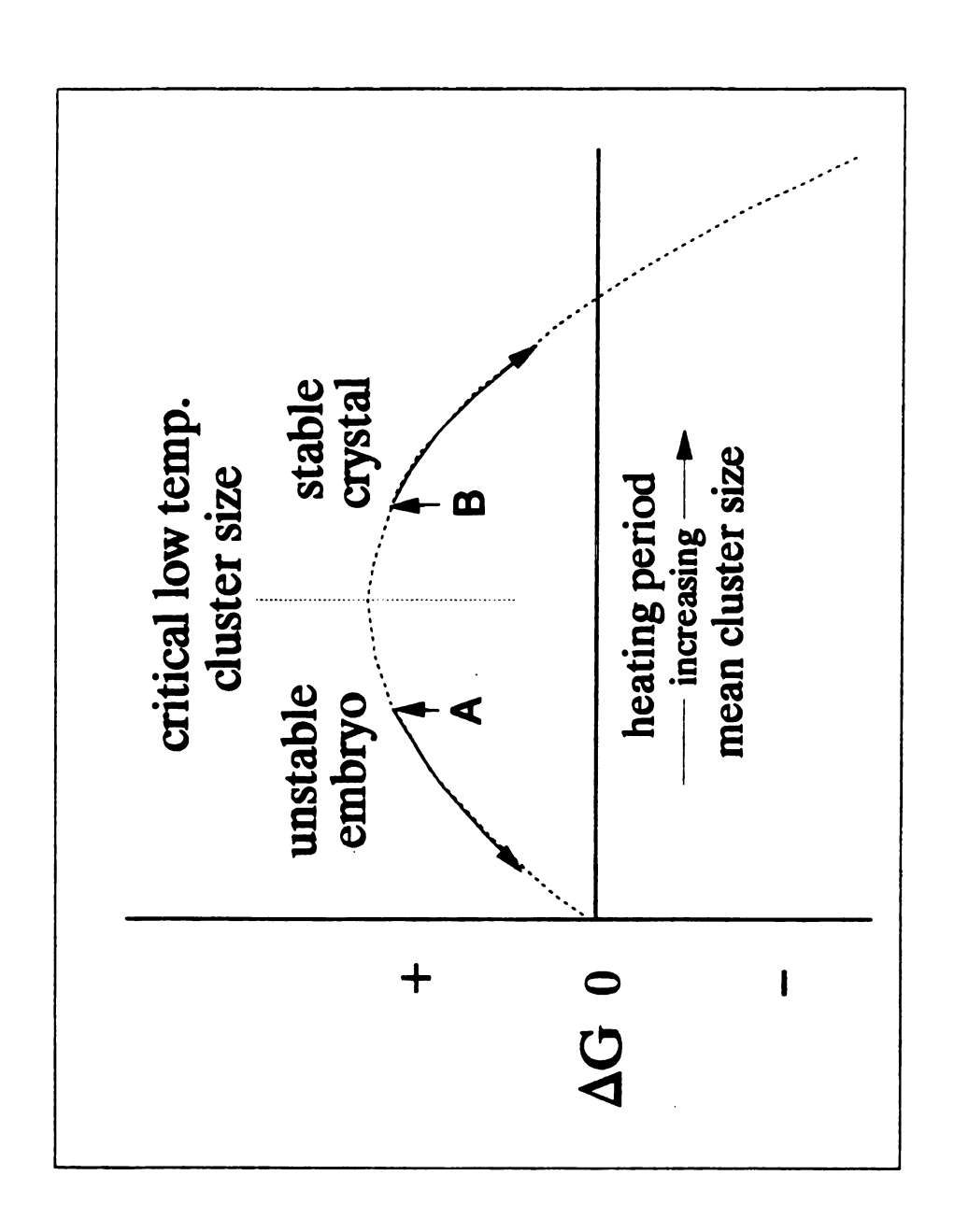
## Nucleation under oscillating temperature

The critical free energy of formation and the corresponding critical radius define a free energy divide that exists in supersaturated solutions. This energy divide may, under conditions used in this study, be used to determine when stable nucleation occurs. The required conditions are: 1) cluster growth rates exceed cluster dissolution rates at high temperatures, 2) subcritical clusters dissolve faster than they grow at low temperatures, 3) supracritical clusters remain stable at low temperatures, and, 4) dissolution of subcritical clusters is rapid at low temperatures. This ensures that significant numbers of subcritical high temperature clusters dissolve at low temperatures within the time parameters of the experiment. Therefore, high temperatures may be used to grow clusters and low temperatures may be used to determine whether they

are subcritical or supracritical on the basis of their tendency to dissolve. In practice, this may be done by comparing the reaction progress as a function of time from isothermal experiments to the reaction progress as a function of the total duration of heating from experiments cycled between high and low temperature. The probability of stable nucleation at high temperature is assumed to increase with the length of the individual heating period. Short heating periods could therefore produce a population of clusters dominated by subcritical clusters that dissolve at low temperatures. As a result of the repeated growth and dissolution of subcritical clusters, significantly more heating time will be needed to accumulate before achieving the same level of reaction progress as is required under isothermal conditions (path A, Fig. 1). If the heating period is long enough to form significant numbers of supracritical clusters, then low temperature dissolution of subcritical clusters will not significantly retard the reaction. As a result, the accumulated heating time from cycled experiments will be the same as the isothermal heating time for the same degree of reaction progress (path B, Fig. 1).

The dependence of cluster stability on the length of the heating period may be used to constrain when and in what order metastable phases nucleate during the conversion of calcite to dolomite. Specifically, most nucleation must occur between the longest heating period that exhibits Figure 1 Generalized thermodynamic stability diagram of hemispherical ion clusters on a planar substrate. The curve presents solutions to Eq. 1 for net free energy (&G) given arbitrary cluster sizes (n) (also see Nielsen, 1964; Berner, 1971). The mean cluster size is assumed to increase with the length of the heating period. The direction of the thermodynamic drive is illustrated for the cases in which stable low temperature nuclei have formed (B) and for where they have not (A).

Figure 1



suppressed nucleation and the shortest heating period that exhibits unsuppressed nucleation. These two limits bracket the time required for critical nucleation. If these dolomitization reactions follow Ostwald's Step Rule because of differences in activation energy, then the length of time required for critical nucleation of each phase should correspond to the order in which each phase appears as a reaction product.

## Experimental Procedure

All experiments used 0.100 grams of reagent grade calcite (Mallinckrodt) and 15 ml of solution in 23 ml Teflon-lined bombs. All of the solutions used, had a Mg:Ca ratio of 0.66 and were obtained by combining two parts of a 1M MgCl<sub>2</sub> solution to three parts of a 1M CaCl<sub>2</sub> solution. The 1M stock solutions were prepared from MgCl<sub>2</sub>·6H<sub>2</sub>O or CaCl<sub>2</sub>·2H<sub>2</sub>O (Baker Analyzed Reagent) dissolved in deionized, distilled water.

The Teflon liners were weighed and 0.1000 (+-.0002) g of Mallinckrodt CaCO<sub>3</sub> added. Fifteen ml of the 0.66 Mg:Ca solution were pipetted into the liner and weighed. The liners were placed into stainless steel Parr bombs and heated at 193° C in a muffle furnace. The temperature within the liners increased rapidly to over 100° C in less then 20 minutes but did not reach 193° C until two hours had elapsed. Most of the heating periods were terminated by cooling the bomb at room temperature for 15 minutes and

quenching it in water. However, several of the experiments were not quenched. The reason for this was that water quenching the experiments using 12 hour heating cycles sometimes resulted in contraction of the retaining spring used to secure the lid of the Teflon vessel. This resulted in slight underpressuring of the lid which lead to an accumulation of small fluid losses that became excessive after 12 or more cycles. Cooling the bombs at room temperature resulted in much less fluid loss.

Reactant loss was determined after each experiment by reweighing the liner plus reactants. An experiment was deemed unusable when reactant loss exceeded 0.52 g, the equivalent of 0.5 ml of solution. The reaction products were filtered, repeatedly washed with deionized, distilled water, and air-dried. Powder smears of the products were made after adding an internal fluorite standard followed by light grinding. The position of the (104) peak relative to the internal fluorite standard was used to determine the MgCO3 content of the solids (Goldsmith et al, 1961; Royce et al., 1971; Lumsden and Chimahusky, 1980). The relative proportions of the reaction products were determined by Xray diffraction methods using peak height ratios of the (104) peak. The (015), (021), and (110) peaks were used to establish the degree of dolomite superstructure ordering (Goldsmith and Graf, 1958; Fuchtbauer and Goldschmidt, 1965).

A series of isothermal experiments at 193° C were used to construct a reaction progress baseline. Two other experimental series were conducted in which heating periods at 193° C were interchanged with 12 hour periods at room temperature. A range of total heating times were obtained by repeating the heating and cooling cycles several times. The first set of these experiments was heated for 12 hour periods, while the second set was heated for 48 hour periods. A third series of reactions involved an initial 48 hour heating period after which the reaction was cycled between 12 hours of heating, and 12 hours of cooling, for a total heating time of 150 hours.

The calculated Mg:Ca ratio of the solution changes from 0.66 to 0.58 during the complete conversion of the calcite reagent to stoichiometric dolomite. This indicates that the reaction takes place in a solution of essentially constant composition. However, cycling the temperature between  $193^{\circ}$  C and about  $25^{\circ}$  C results in significant changes in saturation state that influence the critical radius. The modified van't Hoff equation predicts that the  $\ln \Omega$  in the bombs is about 2.5 times greater at room temperature than it is at  $193^{\circ}$  C. Equation 2 indicates that this would reduce the room temperature critical radius about 2.5 times relative to the critical radius at  $193^{\circ}$  C. However, this is largely offset by the increase in the room temperature critical radius due to the change in temperature.

Recognizing the uncertainties in the value of  $\ln \Omega$ , it appears that the critical radius could actually be somewhat smaller or larger at room temperature than it is at  $193^{\circ}$  C. The fact that, for dolomitization of  $\text{CaCO}_3$ , increasing temperature causes decreasing saturation states ( $\Omega$ ) allows temperature and  $\Omega$  to have a buffering effect. At high temperature, nucleation occurs faster and these fast forming nuclei are preserved at low temperature because  $r^*$  doesn't change very much. Therefore, the reaction products obtained from temperature cycling may be primarily affected by differences in nucleation kinetics.

Most solids increase  $r^*$  with decreasing temperature because decreasing temperature also decreases  $\Omega$ . Therefore, additional growth of high temperature nuclei is needed in most solids so that the drop in temperature does not shift a high temperature nucleus to a subcritical size that results in its dissolution. In this case, our experiments might not be able to separate the kinetics of nucleation from the kinetics of crystal growth.

### Results

Two distinct phases were produced in the isothermal, 12 hour and 48 hour cycled experiments (Table 1). The first phase detected was a high magnesium calcite (HMC) containing approximately 36-39 mole percent MgCO<sub>3</sub>. There were no

ordering peaks associated with this product. The next phase was detected along with HMC and contained 45-48.2 mole percent MgCO3. This is a nonstoichiometric dolomite which produced broad, asymmetric (015) and (021) ordering peaks  $(I(015)/I(110) \approx 0.5)$ . In some cases, two distinct (104) peaks were produced by these two phases. The most stoichiometric dolomite (>48.5 mole % MgCO3) was found only after the calcite reactant and intermediate phases had been completely converted to dolomite. This product produced sharp, symmetric (015) and (021) ordering peaks with a dolomite ordering index (I(015)/I(110)) of about 0.8.

SEM analysis of the products revealed no significant difference in crystal size or morphology based on duration of heating. HMC and nonstoichiometric dolomite both formed smooth-faced rhombs. The surface of the stoichiometric dolomite appeared heavily pitted and corroded. Similar features were interpreted by Katz and Matthews (1977) and Sibley (1990) to reflect dissolution of metastable phases during precipitation of stoichiometric dolomite.

In the isothermal, baseline reactions (Fig. 2 & 3), traces of HMC (37 mol %  $MgCO_3$ ) were first detected after 105 hours of heating. Nonstoichiometric dolomite (48 mole %  $MgCO_3$ ), together with minor quantities of HMC and calcite, were found after 108 hours of heating. After 119 hours, only the more stoichiometric dolomite (>48.5 mole %  $MgCO_3$ ) was found. The results from the 48 hour heating period

experiments were not significantly different (Table 1 and Fig. 2).

The 12 hour heating period experiments produced significantly different results (Table 1 and Fig. 3). As with the baseline and 48 hour experiments, HMC first appeared at 107 hours of total heating. However, seven experiments with heating times ranging from 107 to 240 hours produced no detectable dolomite. In these experiments, the proportion of HMC relative to calcite increased at an almost linear rate from 3% at 107 hours to a maximum of 76 % at 240 hours. Dolomite was found in three runs in this series. The earliest dolomite (46 mole % MgCO<sub>3</sub>) was found at 181 hours of total heating and composed about 16 % of the sample the remainder of which contained HMC and calcite. One experiment had completely converted to stoichiometric dolomite (>48.5 mole % MgCO<sub>3</sub>) after 216 hours of heating.

All four of the experiments involving the 48 hour initial heating period followed by 12 hour heating and cooling periods produced dolomite in 150 hours of total heating. Three of the experiments had gone to completion, producing a near stoichiometric dolomite. One experiment produced HMC and nonstoichiometric dolomite.

TABLE 1

All experiments used 0.100 g CaCO<sub>3</sub> and 15 ml of a 0.66 Mg:Ca, 1M solutions. The heating temperature was at 193<sup>o</sup> C and the cooling period temperature was at room temperature. The length of the cooling period was 12 hrs. for all cycled experiments.

Isothermal Experiments

Sample	Heating Time	20 Cu Ka	Mole Mg	Mole \$ 28 Mg Cu Ka (hrs.)	Mole & & Mg Dol	Do1	# HMC	Prod
I-3	92.50					0	0	0
<u>-</u>	99.75					0	0	0
I-7	100.30					0	0	0
I-10	103.66					0	0	0
I-11	105.63	•	•			0	~	~
I-12	108.20	30.59	37.7			0	17	17
1-9	108.50	•	•	30.95	47.9	28	36	96
1-8	109.50			•	•	100	0	100
H-H	114.25	30.56	36.8			0	<b>5</b> 0	50
I-5	119.50			30.98	•	100	0	100
9-I	126.25			31.02	50.9	100	0	100
I-2	144.00			30.95	•	100	0	100

TABLE 1

(cont)

48 Hour Heating Period

Sample	Heating Time	20 Cu Ka	Mole Mg	Mole \$ 20 Mg Cu Ka (hrs.)	Mole & Mg D	Do1	# HMC	Prod
	109.63	30.52	35.5	30.87	46.3	96 00	<b>24</b> 0	40
	115.50	30.61 30.64	38. 99. 9.3	30.91 30.89	47.6	9 4 4	21	17 55
1 9 - 1 8 - 8 - 8 - 8	119.63 120.50 132.95	30.60 30.56	36.0 36.0	30.85	45.7	0 100	9 20	90 000 000
	133.00	30.64 30.55	39.3 36.5	30.93	48.2	600	0 00 0 00	8 8
	144.23 155.77			30.95	48.8 48.5	100	00	100

TABLE 1

12 Hour Heating Period

Prod	E 2 2 4 9 9 0 1 0 0 0 1 0 0 0 0 0 0 0 0 0 0 0 0
# HMC	E 2 4 0 1 1 2 4 0 7 1 1 2 4 0 7 1 1 2 4 0 7 1 1 2 1 2 1 2 1 2 1 2 1 2 1 2 1 2 1 2
* Dol	1 0 0 0 0 0 0 0 0
Mole &	4 4 4 7 6 9 1 6 9
Mole \$ 28 Mg Cu Ka (hrs.)	30.83 30.87 30.95
Mole Mg	37.7 39.0 30.0 30.0 30.0 30.0 30.0 30.0
20 Cu Ka	00000000000000000000000000000000000000
Sample Heating Time	106.83 107.10 108.60 112.99 112.55 124.73 168.62 180.67 216.50
Sample	1152-13 1152-13 1152-14 12-1-15 12-1-19 11-19

Figure 2 Results of the 48 hour cycled experiments

(triangles and the isothermal baseline (squares).

The reaction products are HMC (open symbols),

mixtures of HMC and nonstoichiometric dolomite

(black filled symbols), and near ideal dolomite

(asterisk filled symbols). Isothermal experiments

in which the XRD response was from calcite

reactant only are designated by asterisks.

Figure 2

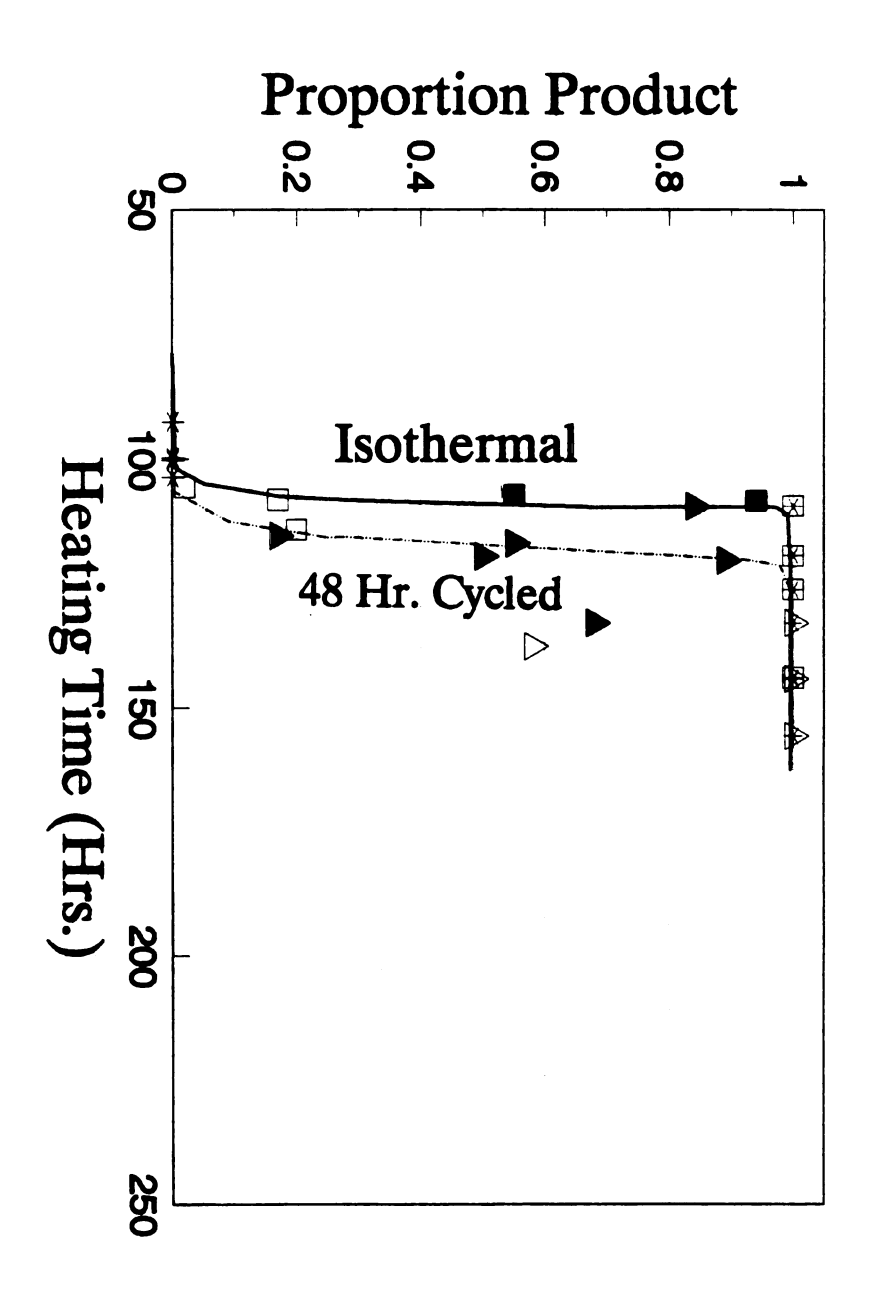
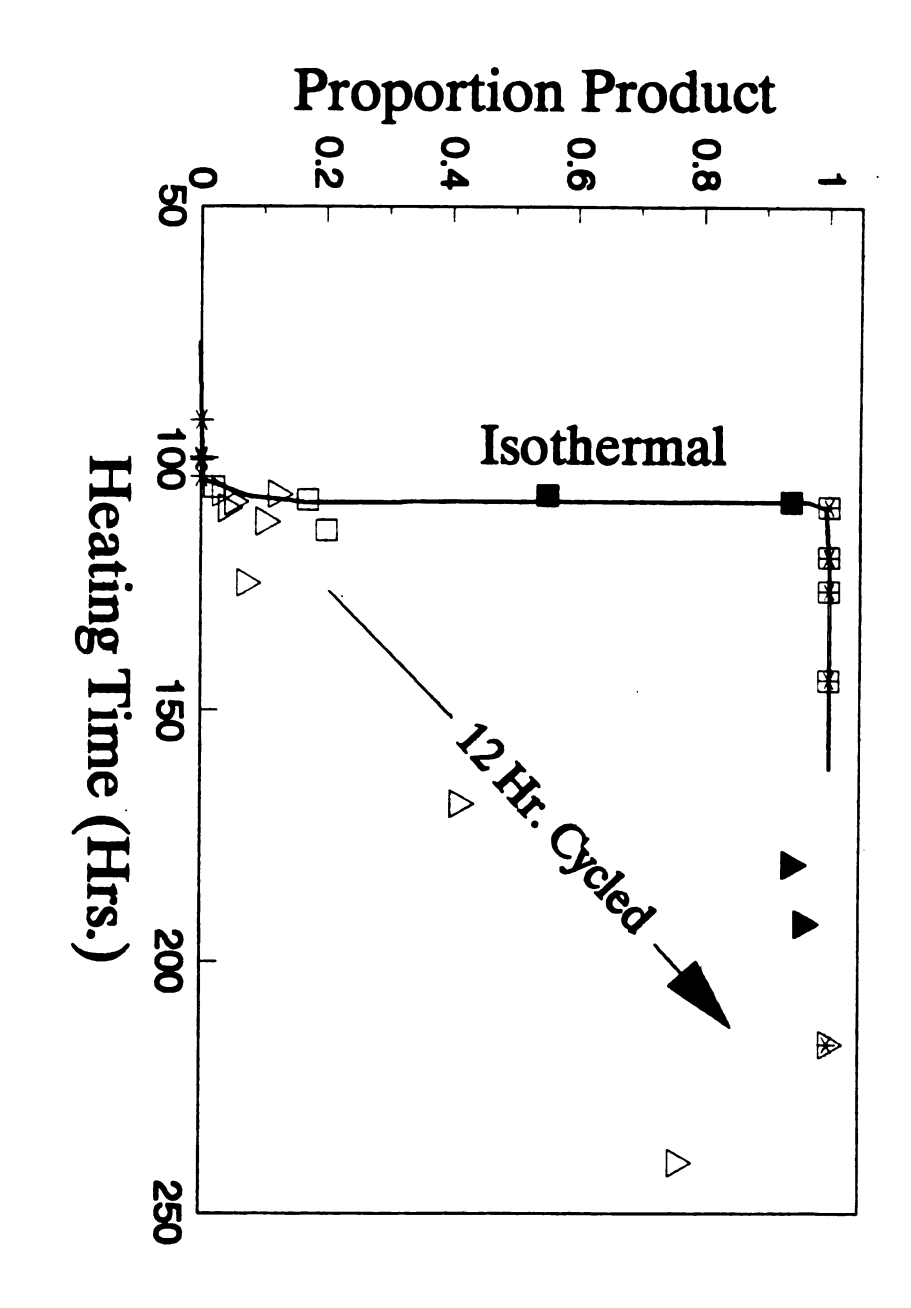


Figure 3 Results of the 12 hour cycled experiments (triangles) and the isothermal baseline (squares).

Other conventions are the same as in Figure 2.

Figure 3



## Discussion

The results indicate that cycling the reaction between high and low temperatures has no detectable influence on the length of time required to form HMC. Furthermore, there is no significant difference in the type of product, its size or morphology. In 12 hour and 48 hour cycled experiments, HMC was first detected between 106 and 109 hours of heating. Because no significant difference was found in the length of the induction period between either of the cycled experiments and the isothermal baseline, nucleation of HMC must occur within the first 12 hours of heating at 193° C. Therefore, the remainder of the induction period reflects HMC crystal growth kinetics.

Nonstoichiometric dolomite first appeared at approximately 110 hours in the baseline and 48 hour cycled experiments but did not appear in the 12 hour cycled experiments until 181 hours of heating. The difference in the apparent induction period for dolomite demonstrates that its nucleation is significantly suppressed by cycling the reaction temperature on a 12 hour period. Furthermore, the experiments using the 48 hour initial heating period demonstrate that the suppression of dolomite nucleation can only be initiated early in the induction period. These results indicate that dolomite nucleation requires more than 12 and less than 48 hours of heating. Furthermore, HMC

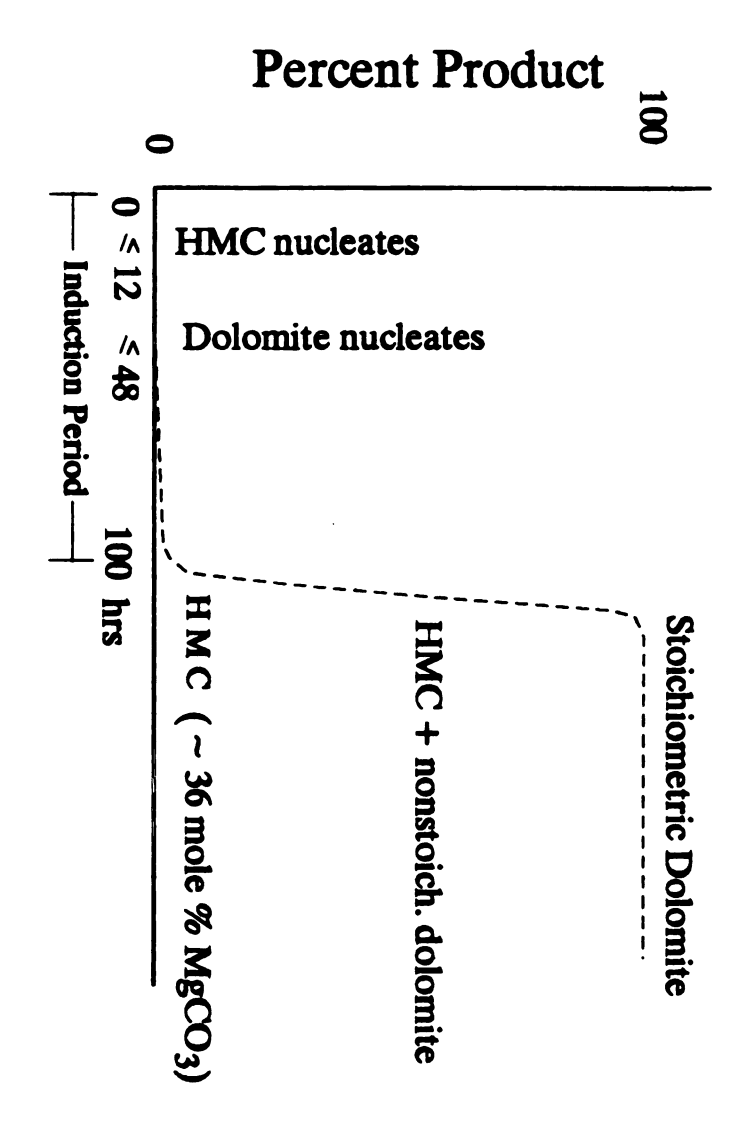
forms stable crystal nuclei before dolomite does, and both nucleate early in the induction period (Fig. 4).

If nucleation rates conform to Eq. 4, then HMC may have nucleated before nonstoichiometric dolomite because its pre-exponential factor (N) is greater than or the activation energy ( $\delta G^*$ ) is less than they are for nonstoichiometric dolomite. If the pre-exponential factor is less important to nucleation than the activation energy, then  $\delta G^*$  of HMC is less then it is for nonstoichiometric dolomite. According to Eq. 3,  $\delta G^*$  is determined by the molar volume, surface free energy and saturation state. Therefore, evaluation of these parameters may provide additional insight into the factors governing the nucleation of HMC and nonstoichiometric dolomite in these experiments.

The molar volume of calcite is approximately one-half that of dolomite (Berner, 1971 and references therein). If the HMC in these experiments has a simple calcite structure and similar molar volume, then HMC nucleation should be favored with respect to dolomite. Therefore, differences in molar volume alone could explain why HMC nucleates before dolomite. Faster HMC nucleation could also be due to its surface free energy coefficient being less than that of dolomite. The saturation state of HMC relative to dolomite favors the nucleation of dolomite. Given these constraints, HMC could nucleate before dolomite when its pre-exponential factor, surface free energy coefficient, molar volume or a

Figure 4 Generalized results of dolomitization
experiments (e.g. Katz and Matthews, 1977; Sibley
et al., 1987; Sibley, 1990; this study). Most of
the reaction time is in the induction period,
during which no products are detected by XRD.
Under the conditions used in this study, HMC
nucleates in less than 12 hrs. of heating while
dolomite nucleates with more than 12 hrs. and less
than 48 hrs. of heating.

Figure 4



combination of these factors is more important than saturation state.

If nucleation kinetics govern the formation of nonstoichiometric dolomite before stoichiometric dolomite because of differences in activation energy then evaluation of the parameters in Eq. 3 indicate that the critical factor is the surface free energy coefficient. Goldsmith et al. (1961) found that the unit cell volume of the dolomite structure decreases as the magnesium content of dolomite increases. Should the molar volume behave in a similar fashion, calcian dolomite should have a larger molar volume than stoichiometric dolomite. When all else is equal, Eq. 3 predicts that the phase with the smaller molar volume should be favored to nucleate first. These experiments indicate that this does not occur. Therefore, differences in molar volume cannot explain why nonstoichiometric dolomite precipitates before stoichiometric dolomite does.

The activation energy is also affected by the saturation state of the solution relative to the two phases. Dolomite solubility increases with the amount of excess calcium in the dolomite structure and decreases with the degree of cation ordering (Carpenter, 1980). SEM analysis of the reaction products shows that earlier and presumably less stoichiometric dolomite commonly exhibited dissolution textures. Therefore, if the final stoichiometric dolomite is less soluble than the nonstoichiometric dolomite, then

solubility differences cannot explain the order in which these phases appear.

The differences in molar volume and saturation state between stoichiometric and nonstoichiometric dolomite both favor stoichiometric dolomite nucleation when differences in the pre-exponential factor are minor. Under the condition of a constant pre-exponential factor, our experimental observations led us to the conclusion that the interfacial free energy coefficient of the dolomite produced in these experiments increases with the magnesium content and/or degree of cation ordering. This is consistent with the general observation that interfacial free energies decrease with increased solubility, and increase with crystal ordering (Steefel and Van Cappellan, 1990). Therefore, the presence of Ostwald's Step Rule in these calcite to dolomite reactions appears to be controlled by molar volume and/or surface free energy-dominated nucleation kinetics.

### Conclusions:

- 1) HMC forms stable nuclei before dolomite at both 193° C and room temperature.
- 2) Nucleation of HMC and dolomite occurs "early" in the induction period at 1930 C.

- 3) Most of the induction period at 193° C involves slow growth of HMC and dolomite crystals. This is followed by a period of rapid growth during which most replacement occurs. The cause of this transition from slow to rapid growth has not been determined.
- 4) Dolomite nucleation is suppressed in these experiments because significant numbers of subcritical clusters formed at high temperature, dissolved within twelve hours at room temperature. This suggests that in order to nucleate dolomite the temperature and/or saturation state that promotes dolomite nucleation must be maintained throughout the nucleation process. However, once nucleation has occurred, these conditions need not be maintained throughout the entire induction period.
- 5) The length of time required to nucleate HMC and nonstoichiometric dolomite is consistent with the order in which these metastable phases appear in the calcite to dolomite transformation at 193° C. Therefore, the adherence of these reactions to Ostwald's Step Rule suggests that nucleation kinetics are an important factor in determining

the formation of metastable phases during dolomitization.

# BIBLIOGRAPHY PART I

- Baker P.A. and Kastner M. (1981) Constraints on the formation of sedimentary dolomite. Science, 213, 214-216.
- Berner R.A. (1971) Principles of Chemical Sedimentology. McGraw-Hill, 240
- Carpenter A.B. (1980) The chemistry of dolomite formation 1: The stability of dolomite. In Concepts and models of dolomitization (ed. D.H. Zenger et al.): SEPM Spec. Publ. 28, 111-121.
- Dunning W.J. (1969) General and theoretical introduction. in *Nucleation* (ed. A.C. Zettlemoyer): Marcel Dekker, Inc. 1-67.
- Fuchtbauer H., and Goldschmidt H. (1965) Beziehungen zwischen calciumgehalt und bilungsbedingungen der dolomite. Geol. Rundsch., 55, 84-101.
- Gaines A. (1980) Dolomitization kinetics. In Concepts and models of dolomitization (ed. D.H. Zenger et al.): SEPM Spec. Publ. 28, 123-137.
- Goldsmith J.R., Graf D.L. (1958) Structural and compositional variations in some natural dolomites. *J. Geol.* 66, 678-693.
- Goldsmith J.R., Graf D.L., and Heard H.C. (1961) Lattice constants of the calcium-magnesium carbonates. Amer. Mineral., 46, 453-457.
- Hardie L.A. (1987) Dolomitization. A critical view of some current views. Jour. Sed. Petrol., 57, 166-183.
- Katz A. and Matthews A. (1977) The dolomitization of CaCO<sub>3</sub>: An experimental study at 252-295° C. Geochim. Cosmochim. Acta, 41, 297-308.

- Lumsden D.N., and Chimahusky J.S. (1980) The Relationship between dolomite nonstoichiometry and carbonate facies parameters, In Concepts and models of dolomitization (ed. D.H. Zenger et al.): SEPM Spec. Publ. 28, 123-137.
- Machel H.G. and Mountjoy E.W. (1986) Chemistry and environments of dolomitization A reappraisal. Earth Science Rev, 23, 175-222.
- Morse J.W., and Casey W.H. (1988) Ostwald processes and mineral paragenesis in sediments. Am. Jour. Sci., 288, 537-560.
- Nielsen A.E. (1964) Kinetics of precipitation, Macmillan, New York, 151 p.
- Royce C.R. Jr., Wadell J.S., and Peterson, L.E. (1971) X-ray determination of calcite-dolomite: An evaluation. Jour. Sed. Petrol., 41, 483-488.
- Sibley D.F. (1990) Unstable to stable transformation during dolomitization. J. Geol., 98, 743-748.
- and Bartlett T.R. (1987) Nucleation as a rate limiting step in dolomitization, in Proceedings, International Symposium on Crystal Growth Processes in the Sedimentary Environment, 2nd, Granada, 1986.

  Madrid, Instituto de Geologica, C.S.I.C., 733-741.
- Dedoes R.E., and Bartlett T.R (1987) Kinetics of dolomitization. Geology, 15, 1112-1114.
- Steefel C.I., and Van Cappellen P. (1990) A new kinetic approach to modeling water-rock interaction: The role of nucleation precursors, and Ostwald ripening.

  Geochim. Cosmochim. Acta, 54, 2657-2677.
- Walton A.G. (1969) Nucleation in liquids and solutions, in Nucleation (ed. A.C. Zettlemoyer): Marcel Dekker, Inc., 225-307.

# PART II

# CONSTRAINTS ON THE RATE-LIMITING STEP GOVERNING DOLOMITE CRYSTAL GROWTH

### ABSTRACT

Surface reaction, diffusion, and reactant supply rates are commonly cited as rate-limiting steps in kinetically controlled reactions. The rate-limiting step may be determined from the thickness and diameter of cathodoluminescent zones of dolomite crystals.

Zone-thickness data were obtained from dolomite crystals in the Burlington-Keokuk (Miss.), Saluda (Ord.), Ft. Payne (Miss.) and Sero Domi (Plio.) Formations. All of the samples had zonation patterns in which the thickness of correlative cathodoluminescent zones were proportional to the average diameter of the crystal at the time the zone formed.

and that the crystal's surface composition and reactant bearing solution were spatially homogeneous, then these data reflect surface reaction limited crystal growth kinetics in which the rate limiting step involves a 2-D nucleation and monolayer growth mechanism. These data may also reflect surface-reaction limited growth kinetics in which nucleation of a calcium-rich dolomite is followed by the progressive addition of less calcian material. This could result in a size dependent reaction rate coefficient and the observed zonation pattern. In order to maintain a spatially constant

solution composition, reactant transport rates must be much greater than crystal growth or bulk dolomitization rates.

The data are also consistent with a model in which nucleation is assumed to be instantaneous, but growth involves spatially inhomogeneous solutions. This inhomogeneity may be caused when bulk dolomitization rates decrease reactant concentrations during transport. The zonation pattern may therefore be explained by bulk reaction rates being of the same order of magnitude as transport rates. If the minimum transport rate is controlled by diffusion then this would indicate that dolomitization rates are not much less than diffusion rates and could be greater.

### Introduction

Dolomite, the thermodynamically favored carbonate mineral in seawater, is very rare in normal marine environments. However, in ancient, environmentally equivalent rocks, dolomite is much more common. One obvious distinction between these two sets of observations is the length of time involved. Therefore, the rarity of dolomite in apparently favorable modern environments is generally explained by a nonspecific reference to kinetics. In the transformation of calcite or aragonite to dolomite, the kinetically slow step may involve dolomite nucleation rates and/or crystal growth-rates. This study is concerned with evaluating the relative importance of surface-reaction rates and reactant-transport rates to the kinetics of dolomite crystal growth as exemplified by cathodoluminescent zonation patterns.

Surface-reaction-limited kinetics has been shown to limit the rate of calcite precipitation (Morse 1983).

Because calcite is the closest analog to dolomite in terms of composition and structure and because it precipitates readily under laboratory conditions while dolomite does not, it may be argued that dolomite growth is also surface-reaction-limited. This is consistent with Reeder and Prosky's (1986) and Fouke and Reeder's (1992) studies in which unequivalent crystal faces were found to grow at different rates and with different compositions. The

presence of two distinct compositional faces on the same crystal requires that at least one face not be at equilibrium with the solution, thus indicating that crystal growth was limited by surface-reaction rates. In order for surface-reaction kinetics to limit dolomitization, the rate of reactant supply must exceed the surface-reaction rate. Several factors may be involved in either inhibiting or promoting surface-reaction rate limited dolomitization. Dolomitization rates may be increased by concentrating reactants in the dolomitizing fluid by evaporating seawater, continental-meteoric waters or mixtures of these (Butler 1969: Pierre et al. 1984; Mazzulo et al. 1987; Warren 1990). Dolomite supersaturation may also be increased by precipitating gypsum, thereby increasing the dissolved Mg/Ca ratio, or by increasing the carbonate alkalinity of the solution by microbial reduction of sulfate (Butler 1969; Compton 1988; Middelburg et al. 1990). Reduced dolomitization rates have been found when traces of dissolved sulfate are present (Baker and Kastner 1981).

Dolomitization may be limited by reactant supply because insufficient  $Mg^{2+}$  is present in most carbonate sediments to account for the amount of dolomite commonly found in ancient carbonate rocks. Therefore,  $Mg^{2+}$  must have been supplied by some source external to the sediment itself. In these situations, the source of  $Mg^{2+}$  is often some distance from sites of active dolomitization so that dolomitization rates may be limited by the rate at which

Mg<sup>2+</sup> is transported into and through the sediment to the site of dolomitization. Therefore, diffusion, advection or a combination of these processes may be important in dolomitization (Machel and Mountjoy 1986).

Chemical gradients in pore-waters adjacent to deep sea dolomites suggest that diffusion rates could limit dolomitization by restricting supplies of one or more reactants (Baker and Burns 1985; Compton 1988; Middelburg et al 1990). Typically, diffusion rates are orders of magnitude less than advective flow rates. As such, diffusion may be considered the slowest rate possible in solute transport. Even where macroscopic advective fluxes supply the bulk solution with reactants, diffusion may, on the microscopic scale, still be operative (Pingatore 1976).

In this study we present data that constrains the mechanism that limits dolomite crystal growth. A simple pattern of crystal growth was found in all four locations studied. Simply said, this pattern reflects a situation in which small crystals grow slower than large crystals.

Mechanisms responsible for such a pattern are limited to one of two possible surface-reaction limited processes when continuously nucleated crystals grow in homogeneous solutions. These data are also consistent with crystal growth in which there are spatial variations in reaction kinetics. Such variation could be induced by bulk reaction rates that are about the same order of magnitude as solute transport rates. If so, dolomite crystal growth rates may

not be much less than the minimum rate of reactant transport governed by diffusion.

### Crystal Growth

The rate-limiting step in dolomite growth may, under appropriate conditions, be deduced from measurements of cathodoluminescently (CL) zoned crystals. Kretz (1974) and Carlson (1989) developed the concepts used in this study to determine the rate-limiting step in the growth of compositionally zoned garnets. These studies were premised on the idea that the rate-limiting step in crystal growth imposes an algebraic relationship between a crystal's radius and the thickness of some compositional zone. The algebraic relationship derived from measurements of crystal radius and zone thickness may be used with theoretical crystal growth laws to constrain the rate-limiting step. Kretz (1974) and Carlson (1989) showed that this could be done when crystals continuously nucleate and grow from solutions with compositions that vary in time but not in space. As a result, compositionally zoned crystals of different sizes are formed in which common compositional zones record crystal growth over equivalent periods of time. The width of a single compositional zone therefore provides a measure of crystal growth rate (dr/dt) which, depending on the ratelimiting step controlling crystal growth, may vary as a function of crystal radius.

Rates of crystal growth from solution may be limited by reactant flux or surface-reaction rates. Because flux and

surface-reaction rates are serial processes, mass balance considerations require that overall crystal growth rates be determined by the slower process. Kretz (1974) and Carlson (1989) considered the endmember processes of pure surface-reaction-limited growth and diffusion-limited growth under the conditions of constant nucleation and precipitation from spatially homogeneous solution.

### Surface-Reaction-Limited Growth

When surface-reaction rates are slower than the capacity of the solution to deliver reactants or remove products, crystal growth depends on the the free-energy difference (delta G) between the solid phase and the solution. This is reflected in the saturation state of the crystal with respect to the solution. The probability of an appropriate ion arriving at a potential growth sites on a crystal increases with saturation state, thereby enhancing growth rates. The ease of attaching solute to the surface is dependent on the density and the molecular geometry of growth sites. Depending on the number of adjacent molecular units bounding a growth site, ions may attach by forming one or more bonds with these adjacent units. The stability of the attachment and the free-energy released will increase with the number of bonds formed.

Crystal-growth mechanisms may be discriminated on the basis of how growth sites are formed and propagated. One

class of growth models involves a surface-nucleation step followed by the addition of solute to the edge of a single crystal monolayer. Growth may also involve dislocation-controlled growth where ions are added to a spiral of monolayers centered on some form of screw dislocation (Burton, Cabrera, and Frank 1951; Nielsen 1964). This configuration provides a continuous source of growth sites thus eliminating the surface-nucleation step.

### 2-D Nucleation-Monolayer Growth

Surface nucleation followed by growth of monolayers are the general features of 2-dimensional nucleation and growth The interaction of surface-nucleation rates and models. layer-growth rates may be used to describe a variety of growth laws. Typically, the energetics of nucleation are greater then the energetics of layer growth. This is because surface nucleation requires overcoming a surface energy that hinders formation of stable nuclei from clusters of ions. Once a surface nucleus achieves a minimum size, by bonding a critical number of ions, it will be stable. As a result, the probability of achieving a critical number of ions under isothermal conditions is controlled by solution composition and surface area available for nucleation. When saturation states are high, the probability of ions arriving and bonding at some nucleation site is greater than at low saturation states.

After stable nucleation, ions may be added to the margin of a spreading monolayer of ions. Expansion of the monolayer continues until impeded by either reaching a crystal edge or a dislocation. In general, adding ions to steps formed on the edge of a spreading monolayer requires less energy than nucleation. Situations may exist in which this is not true, such as when growth sites are filled by foreign ions acting as reaction inhibitors. Obviously, a variety of growth laws are needed to describe the interaction between all possible nucleation and monolayer growth rates. For the sake of simplicity, only the end member cases of mononuclear and polynuclear growth will be considered here.

### Mononuclear layer growth

Mononuclear layer growth results when surface nucleation rates are much less than layer growth rates. Consequently, crystal growth is controlled only by surface nucleation rates because each surface nucleation adds a new layer to the crystal before the next nucleation occurs. When the solution composition is constant, surface nucleation will depend only on surface area. Therefore, the rate at which ion layers are added to the crystal will be a function of surface area and time. Under conditions of

constant crystal shape and solution composition, growth will follow: (Nielsen 1964; Ohara and Reid 1973):

Eq. 1 
$$dr/dt = kr^2$$

where k is a function of surface and bulk solution composition, diffusion coefficient and width of the mononuclear layer. The mononuclear growth rate obviously increases as the crystal grows so that at some point it may no longer be rate-limiting. In this situation, diffusion or another surface-reaction mechanism may limit further growth.

### Polynuclear Layer Growth

Crystal growth ma be accomplished through the addition of surface nuclei only. This is the polynuclear model in which surface nuclei with constant area and thickness form but do not spread. As a result, any one mononuclear layer consists of a specific number of adjacent surface nuclei. If the nucleation rate is linearly dependent on surface area then coverage by a single monolayer will occur at a constant rate so that the radial rate of crystal growth follows (Nielsen 1964):

Eq. 2 
$$dr/dt = k$$

The rate constant k is again a function of surface and bulk solution composition, diffusion coefficient, crystal surface area and mononuclear layer width.

### Screw Dislocation Limited Growth

Screw-dislocation-limited growth eliminates the nucleation process by propagating an Archemedian spiral of monolayers centered on a screw dislocation (Burton, Cabrera and Frank 1951). Growth is accomplished by adding ions to a continuous source of steps formed by the edge of the spiral. As the crystal grows the monolayer migrates outward from the dislocation so that the position of the steps rotate about the dislocation. Under conditions of constant solution composition, the rate of spiral rotation is constant, so that adjacent turns of the spiral maintain a constant distance. In the limit of a sufficiently large spiral, the number of potential growth sites per unit area approaches a constant value. This results in a crystal growth rate that may be approximated as (Neilsen 1964):

### Eq. 3 dr/dt = k

### Diffusion limited growth

Reactant flux rates limit crystal growth when surface-reaction rates exceed the solution's capacity to deliver reactants. Crystal growth, when limited by reactant flux rates, becomes dependent upon diffusive and advective

transport. In the absence of advection, crystal growth may be described by Fick's first and second laws of diffusion.

Eq. 4 J = -D grad C

Eq. 5  $\frac{dC}{dt} = D \operatorname{div} C$ 

where the flux (J) is the amount of solute diffusing down a concentration gradient through a unit area normal to the gradient. This flux is determined by the diffusion coefficient (D) and concentration gradient (grad C). change in the reactant concentration in the solution with time is given by Eq. 5 in which div C is the Laplacian differential operator. According to Nielsen (1964), an analytical solution may be obtained for spherical crystals when growth establishes a steady-state concentration gradient about the crystal. In this situation dC/dt in Eq. 5 is zero so that the radial rate of crystal growth (dr/dt) is equal to the reactant flux (J) that becomes crystalline volume. The appropriate conversion factor is given by the molar volume (v). The flux of reactants is given by the product of the diffusion constant (D) and the change in concentration over distance (dC/dl). Defining the distance in terms of the crystal's radius (r) yields an expression in which the rate of crystal growth is a function of reactant flux in terms of crystal size:

Eq. 6 
$$dr/dt = v J = v D (dC/d1)_{1=r} = v D(C_{inf}-C_s)/r$$

where dC/dl is the reactant concentration gradient, r is the radius of the crystal at time t, and  $C_{inf}$  and  $C_{s}$  are reactant concentrations at infinity and the crystals surface respectively. When the parameters in the numerator of Eq. 6 are held constant and defined as k, diffusion-limited growth becomes:

### Eq. 7 dr/dt = k/r

All of the rate laws considered to this point hold that contemporaneous precipitation is of identical composition on all crystals. Furthermore, the solution from which precipitation is taking place is taken to be compositionally homogeneous with respect to whatever constituents are producing the measured zonation. As a result, the difference in crystal size as a function of time is dependent solely upon the nature of the growth mechanism and the age of the crystal.

TABLE 1

# Rate-Limiting Step Rate Law I. Surface-Reaction Limited A) Mononuclear Growth dr/dt = k r<sup>2</sup> B) Polynuclear or Dislocation dr/dt = k C) Screw Dislocation Limited dr/dt = k II. Diffusion-limited Growth dr/dt = k/r

Table 1 summarizes the rate-limiting steps and the associated growth rate laws that may be encountered when isolated crystals precipitate from spatially homogeneous solutions. In these growth laws r is the crystal radius, k is the growth rate coefficient and t is the length of time the crystal grows. The conditions of constant crystal and solution composition simply reflect precipitation under conditions of constant free-energy change or spatially constant reaction kinetics.

### Methods

### Crystal zone measurements

The data in this study were obtained from measurements made on photomicrographs of cathodoluminescently zoned dolomite crystals. Color slide film was used with a Nuclide ELM-2 lumoscope operating at about 100 millitorr vacuum, with the beam voltage at 14-18 kv and current of 0.5 ma. Measurements were taken from the slides using a low power binocular scope equipped with a graduated reticule. In order to obtain a consistent set of measurement data the following criteria were established.

- 1) Zones must be clearly identifiable.
- 2) This zone must be present in other crystals within the thin-section.
- 3) Zones occurring on crystal edges are unusable.
- 4) Measurements must use centrosymmetrically zoned equilateral rhombs.
- 5) An additional zone, internal to the zone being measured must be present.

For each crystal that appeared to conform to these criteria, measurements were made of A, B, M1-M4, and M2-M3 (see Fig. 1).

### Geometric Correction

The processing of these data involved a geometric correction based on the assumption that the dolomite crystals in this study are unit rhombs in which the interfacial angle is 730 15' and that the CL zonation is morphologically concentric. The presence of a zone internal to the zone of interest assures that measurements are made on crystals that have been cut completely through the zone of interest and at least as close to the morphologic center of the crystal as the internal zone. The presence of centrosymmetric zoning in an equilateral form would therefore indicate that the cut is also subparallel to a crystal face. From these assumptions a geometric correction can be made when the acute interior angle of the apparent equilateral rhomb is less than 73° 15' (See Fig. 1). The correction involves trigonometrically rotating the rhomb about an axis extending between the two acute interior angles. If the acute angle is greater than 73° 15', then no correction is required because rotation about an axis coincident with the direction of measurement involves no displacement. The measurements A, B, M1, M2, M3, and M4 (Fig. 1) were used to construct the triangle A, B, C, (Fig. 2). From this triangle, deviation from an equilateral rhomb

Figure 1 Schematic diagram of a CL zoned crystal showing the zone of interest in light gray and an internal zone in dark gray. A and B are measurements of the exterior edge of the zone of interest. Measurements E and C are the crystal diameters corresponding to the internal and external perimeters of the zone.

Figure 2 Triangle constructed from measurements in Fig. 1 used to find  $\tau$ , E' and C' when B is less than 73° 15'.

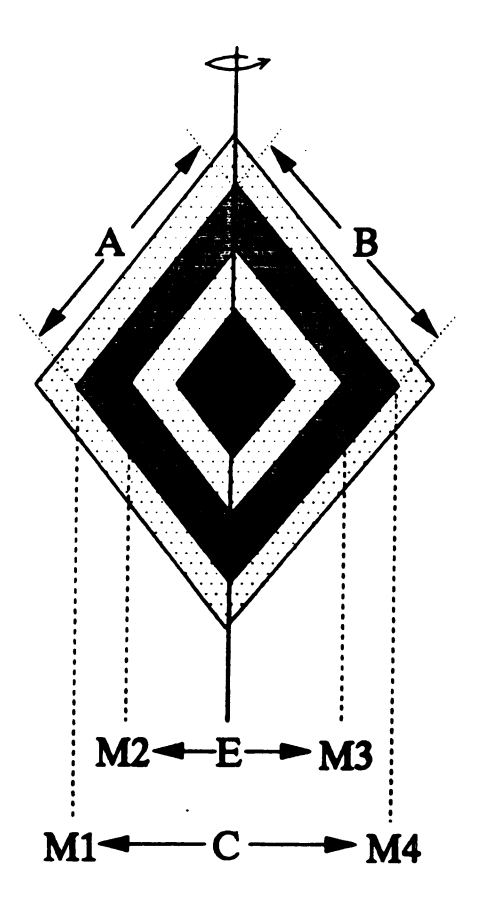


Figure 1

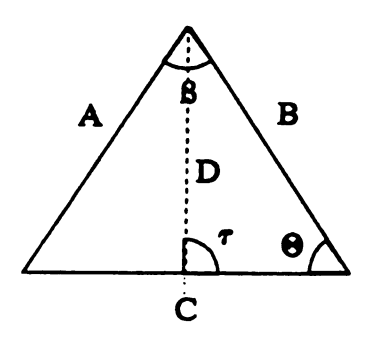


Figure 2

was determined by finding the angle  $\tau$  from:

Eq. 8 
$$\tau = \cos^{-1} \left[ \frac{[1/2(A^2-B^2)]}{[1/2(B^2+A^2-[C^2/2])^{1/2}C]} \right]$$

If  $\tau$  was not within +/- 5° of 90° then the crystal measurement was not used. The corrected diameter of the outside perimeter of the zone of interest (C') was found with:

Eq. 9 
$$C' = [2(B^2+A^2-C^2/2)]^{1/2} \text{ Tan } (1/2[73^{\circ} 15'])$$

and the corrected diameter extending between the inside perimeter of the zone (E') was found with:

Eq. 10 
$$E' = E C'/C$$

The corrected zone thickness (ZT) provides a measure of crystal growth rate and is given by:

Eq. 11 
$$ZT = (C'-E')/2$$

The average crystal radius over which this growth rate operated is given by the corrected crystal radius (CR) measured from the center of the apparent rhomb to the midpoint of the zone that corresponds to ZT or:

Eq. 12 
$$CR = (E'+ZT)/2$$

### Data Normalization

Corrected measurements of zone thickness and radius were normalized to the largest and presumably oldest or fastest growing crystal in a given data set. The various radii (CR) were normalized to the largest crystal radius (CR\*) as follows (Kretz 1976):

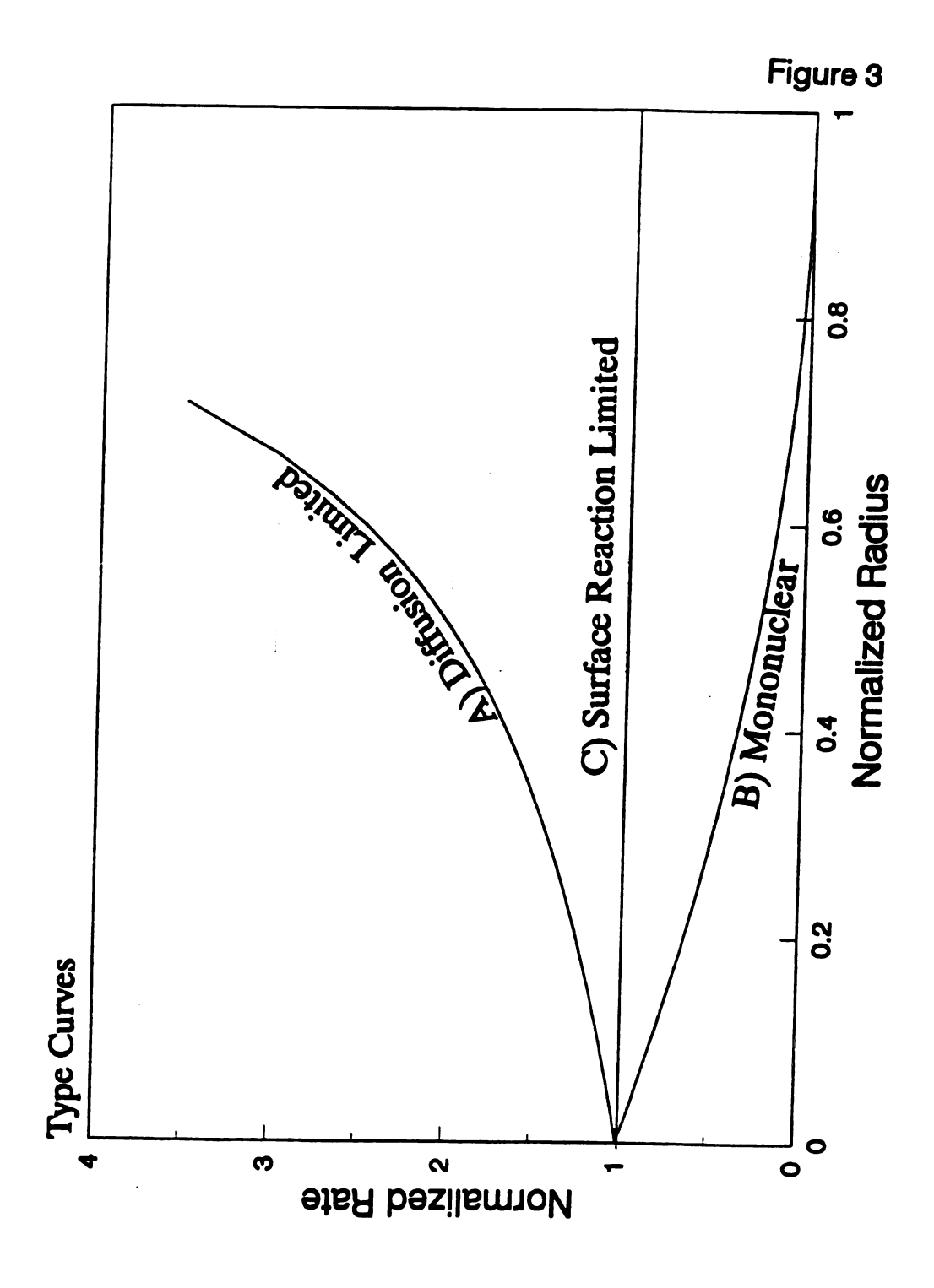
Eq. 13 Normalized Radius = 
$$1-(CR/CR^*)$$

and the various zone thicknesses were normalized to the corresponding zone thickness  $(ZT^*)$  of the largest crystal as follows (Kretz 1976):

## Eq. 14 Normalized Rate = ZT/ZT\*

This normalization follows Kretz (1976) and Carlson's (1989) procedure, so that the resulting type curves are equivalent. Curves A, B and C in Fig. 3, are the normalized type curves for diffusion-limited, mononuclear, and surface-reaction-limited (polynuclear or spiral-dislocation-limited) growth respectively.

Figure 3 Type curves for the normalized growth laws considered in this study. Curve A is the radius-rate relationship expected for diffusion-limited growth (dr/dt=k/r). The endmember conditions for surface-reaction-limited growth are given by curves B and C. Curve B is for mononuclear growth (dr/dt=kr²) and Curve C is for polynuclear or spiral-dislocation limited growth (dr/dt=k). Line D is the expected radius-rate relationship in which growth involves either a size dependent reaction coefficient (dr/dt=kr) or spatial variations in growth kinetics (normalized radius = normalized rate). After normalization, k=1 in the above rate laws.



### Sample characterization

### Seroe Domi

The lower Seroe Domi Fm. (Pliocene) is a completely dolomitized coralline algal grainstone to wackestone which is in some locations at least 20 meters thick and extends 75 km across the Netherlands Antilles (De Buisonje 1974). The variation in thickness is due to the irregularities of the underlying and overlying unconformities. The Seroe Domi dolomites are composed of Ca- rich planar cements and fine crystalline replacement of micrite and mimetic replacement of coralline algae. Cathodolumiscence zoning is found in most dolomite crystals in the lower Seroe Domi. The zoning can be correlated between crystals at an individual outcrop but not between outcrops as little as 1 km apart.

The  $\delta^{18}$ 0 of the dolomites range from 0.5 to +4.0 per mil (Sibley 1980; Lucia and Major in press). These data are consistent with the hypothesis that the dolomite formed from refluxing hypersaline brines (Sibley 1980; Lucia and Major in press). Other geochemical data and petrographic relationships between the dolomite cements and precursor calcite cements are consistent with dolomitization in mixed waters (Sibley 1980; Staudt et al. 1993).

### Burlington-Keokuk

The Burlington-Keokuk formation is a 60-90 m thick, regionally extensive carbonate sequence that crops out in eastern Iowa, western Illinois, and northwestern Missouri. It lies unconformably on Kinderhookian rocks and is conformably overlain by the Warsaw Shale or unconformably overlain by Middle Pennsylvanian rocks. Deposition of the Burlington-Keokuk appears to have been in shallow-water on a broad intracratonic shelf (Carlson 1979). The locales sampled probably represent various mid-shelf facies in which sedimentation was continuous and subtidal. Three episodes of dolomitization have been distinguished on the basis of trace-element composition and cathodoluminescence (Cander et al. 1988). The earliest dolomite is often cathodoluminescently zoned and appears to have formed shortly after deposition at less than 500 m of burial (Cander et al. 1988; Kaufman et al. 1988; Banner et al. 1988, Banner et al. 1988a). Cathodoluminescent zones in the earliest dolomite are correlative on the outcrop scale but not beyond (Cander et al. 1988). Choquette et al. (1991) found that this dolomitization selectively replace lime-mud, even at very small scales. Based on isotopic evidence, Banner et al. (1988) proposed that the earliest dolomite formed from predominantly marine waters mixed with meteoric waters. The meteoric waters may have been derived from recharge areas along the transcontinental arch during periods of emergence represented by the unconformities

between the Salem and St. Louis Limestones (Meramecian) and between the Mississippian and Middle Pennsylvanian (Banner et al. 1988).

This study is restricted to the earliest cathodoluminescently zoned dolomite, samples of which were collected from the Biggsville quarry in Henderson County, Illinois and the Harper quarry in Keokuk County, Iowa. The section exposed at the Biggsville quarry consists of a series of generally upward-shoaling sequences of largely undolomitized, massive grainstones, partially dolomitized wacke-packstones and thinly bedded dolostones. In a few of these units nodular chert is a common constituent . Samples were collected above a terrace cut about 10 m below the unconformity between the Burlington-Keokuk carbonates and Pennsylvanian clastics. Samples BV-23, BV-25 and, BV-4 were collected about 1 m, 3 m and 10 m below this contact respectively. The same general depositional pattern was found in the Harper Quarry. At this location samples HS-1, H-2, H-3 and H-4 were collected at about 0.5 meter intervals extending upsection from the base of a 2 m exposure along the quarry's access ramp.

# Ft. Payne

The Fort Payne formation was sampled near Jellico, Tennessee at an extensive exposure along Interstate I-75. The exposure contains Mississippian- aged rocks ranging upwards from the Borden shale through a carbonate section capped by terrigenous clastics. The Fort Payne is the basal carbonate in this section and is separated from the Borden by a thin green glauconitic shale known as Floyds Knob Bed. The Fort Payne is about 20 m thick with the bottom 10.5 m composed of dolomite and cherty dolomite. Proceeding upsection, the Ft. Payne becomes increasingly silty and less dolomitic. Near the top, dolomite all but disappears in favor of crinoidal grainstone to wackestone lenses within a dark gray silty shale. The wide variety of facies found in the Ft. Payne suggests a complex depositional history. BeMent et al. (1981) interpreted the Ft. Payne, in the Jellico area, as a generally shoaling upward sequence formed under shallow intertidal to supratidal conditions. and Elkins (1974) found chert geodes containing anhydrite cores elsewhere in the dolomitized section of the Fort Payne and suggested that dolomitization may have involved evapoconcentrated brines associated with a prograding arid shoreline.

#### Saluda Formation

A 22 m section of the Saluda Formation, exposed in a roadcut on U.S. Highway 451 approximately two miles North of Madison Indiana was sampled. It is a massive Ordovician aged dolomite unit that caps the generally upward shoaling Cincinnati Group (Brown and Linebeck 1966). Near Madison, the contact between the interbedded shales and limestones of the Dillsboro Formation and the overlying Saluda Formation is placed at the base of the first dolomite (Brown and Linebeck 1966; Hatfield 1968). A 8 m thick tempestite section containing thinly interbedded and laterally discontinuous fossiliferous grainstones and lesser amounts of dolomicrite is found between the base of the Saluda and a 2 m thick section of bioturbated dolomite. This unit contains the large spherical corals (Tetradium) characteristic of the Saluda (Hatfield 1968) and is capped by a possible algal laminate. The remaining 16 m of the Saluda is sparsely fossiliferous and is comprised of massive to thinly laminated dolomite. This is disconformably overlain by normal marine limestones of the Whitewater Formation (Brown and Linebeck 1966; Hatfield 1968).

The Saluda Formation is a broad biconvex lens of various lithologies that principally include dolomite. It outcrops in southeast Indiana, southwest Ohio and northern Kentucky. Hatfield (1968) interpreted the Saluda to represent deposition in a lagoonal environment largely

isolated from open marine conditions by small topographic highs associated with accumulations of coral. Within the lagoon, evaporation of sea-water may have formed penesaline to hypersaline solutions that acted as the primary dolomitizing fluids during deposition and shallow burial of lagoonal lime muds (Hatfield 1968, Martin 1978).

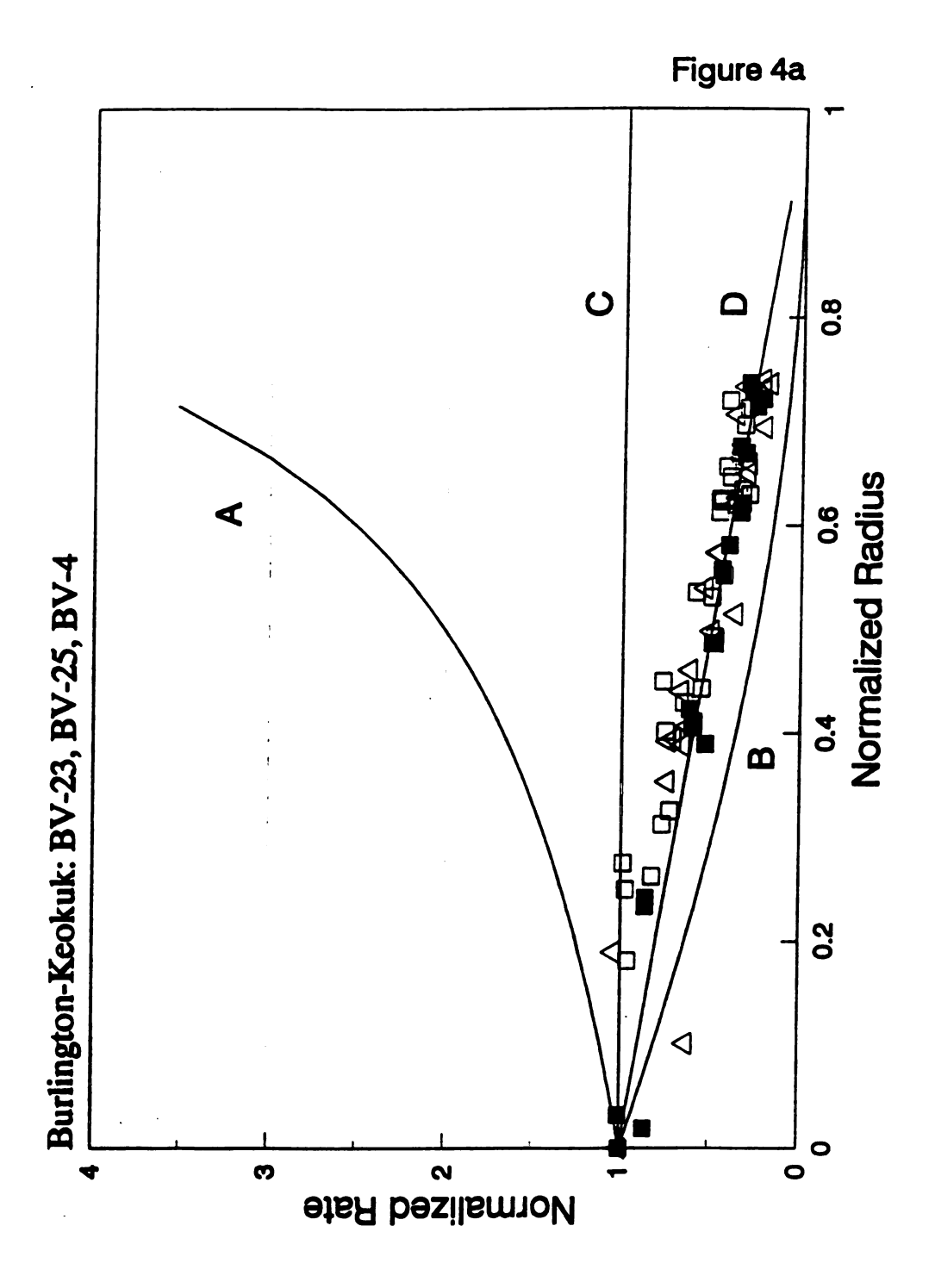
### Results

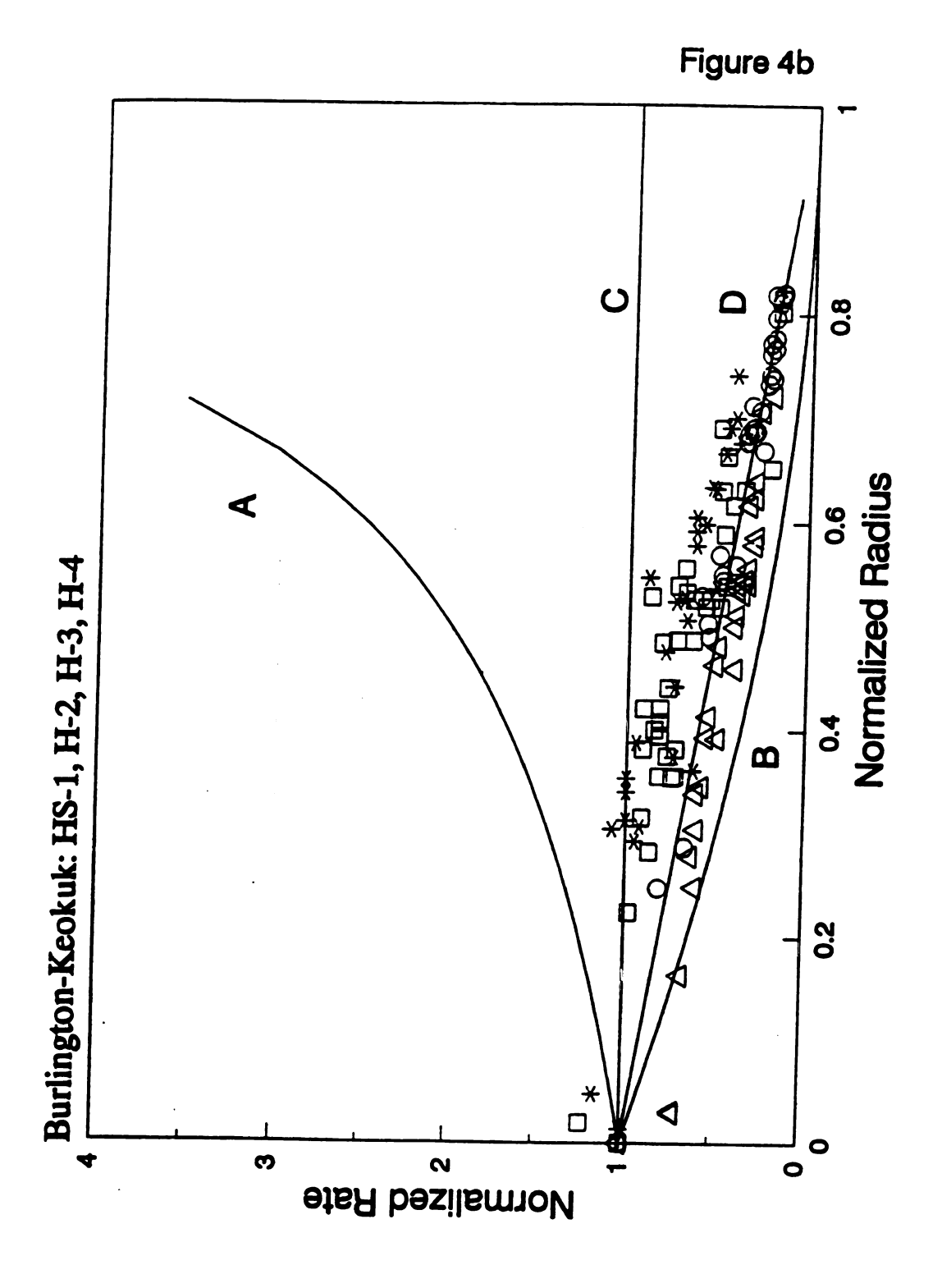
The radius-rate plots for all of the samples in this study have significant numbers of data falling on one or possibly two linear trends. In all of the thin-sections analyzed, most of the data fall along line D. In thinsections BV-4, H-4, SC 34-E, Sal-5 and M-9 all of the data, from the largest crystal to the smallest (Figs. 4a,b,c,e) trend along this line. The remainder of the samples contain at least a few data that fall on the line (C) for surfacereaction-limited growth. This behavior is especially apparent for samples HS-1 and H-2 (Fig. 4b). Radius-rate behavior consistent with the surface-reaction-limited line is restricted to the larger crystals within a given thinsection. However, these data may simply reflect variation about line D as it converges with line C. No significant difference was found in the radius-rate trends between locales within a single formation or between formations. The data are inconsistent with either the diffusion-limited or mononuclear-limited growth laws (Cases Ia or II of Table 1).

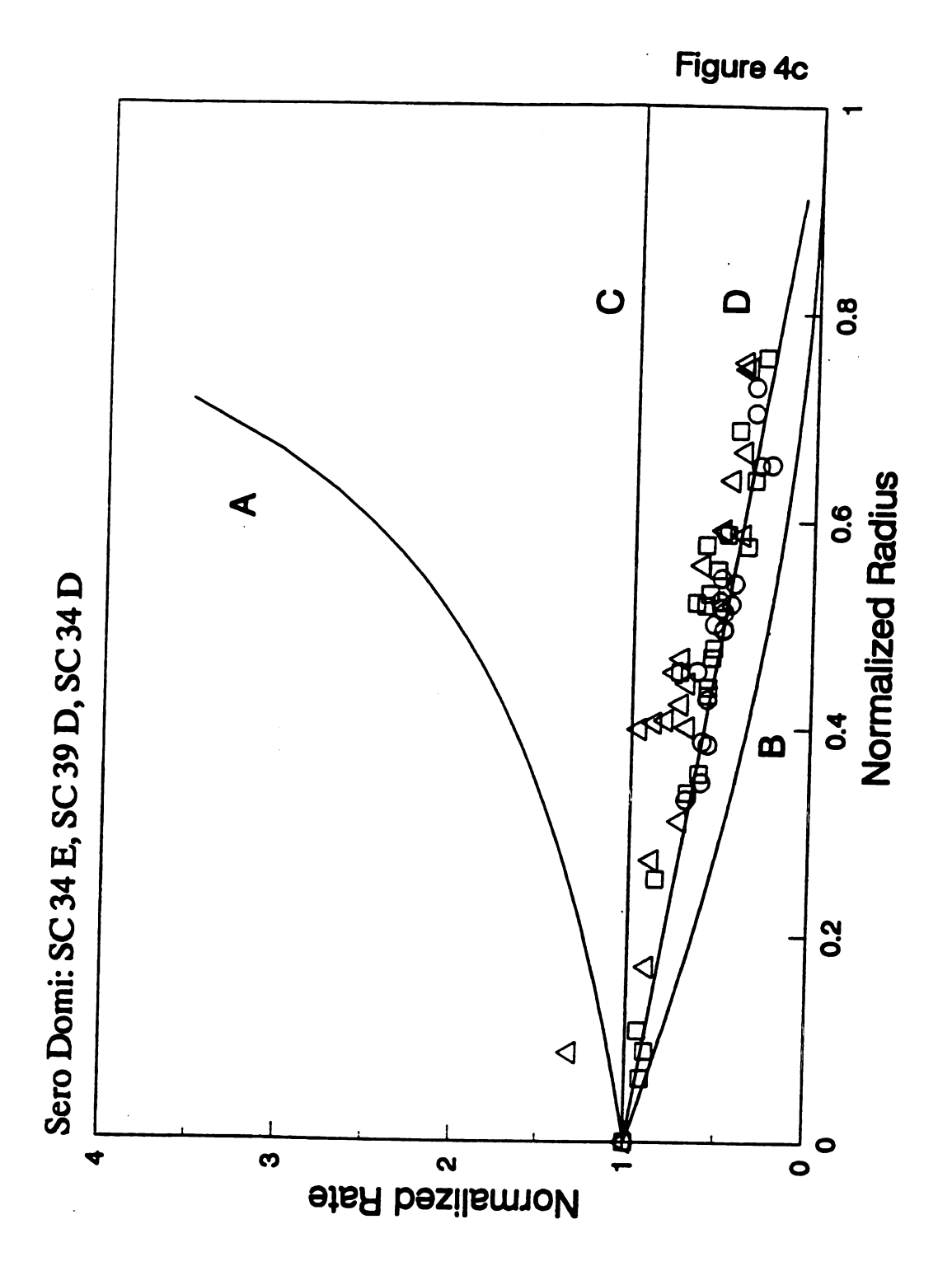
Figure 4 Normalized radius-rate data plotted on the type curves from Fig. 3.

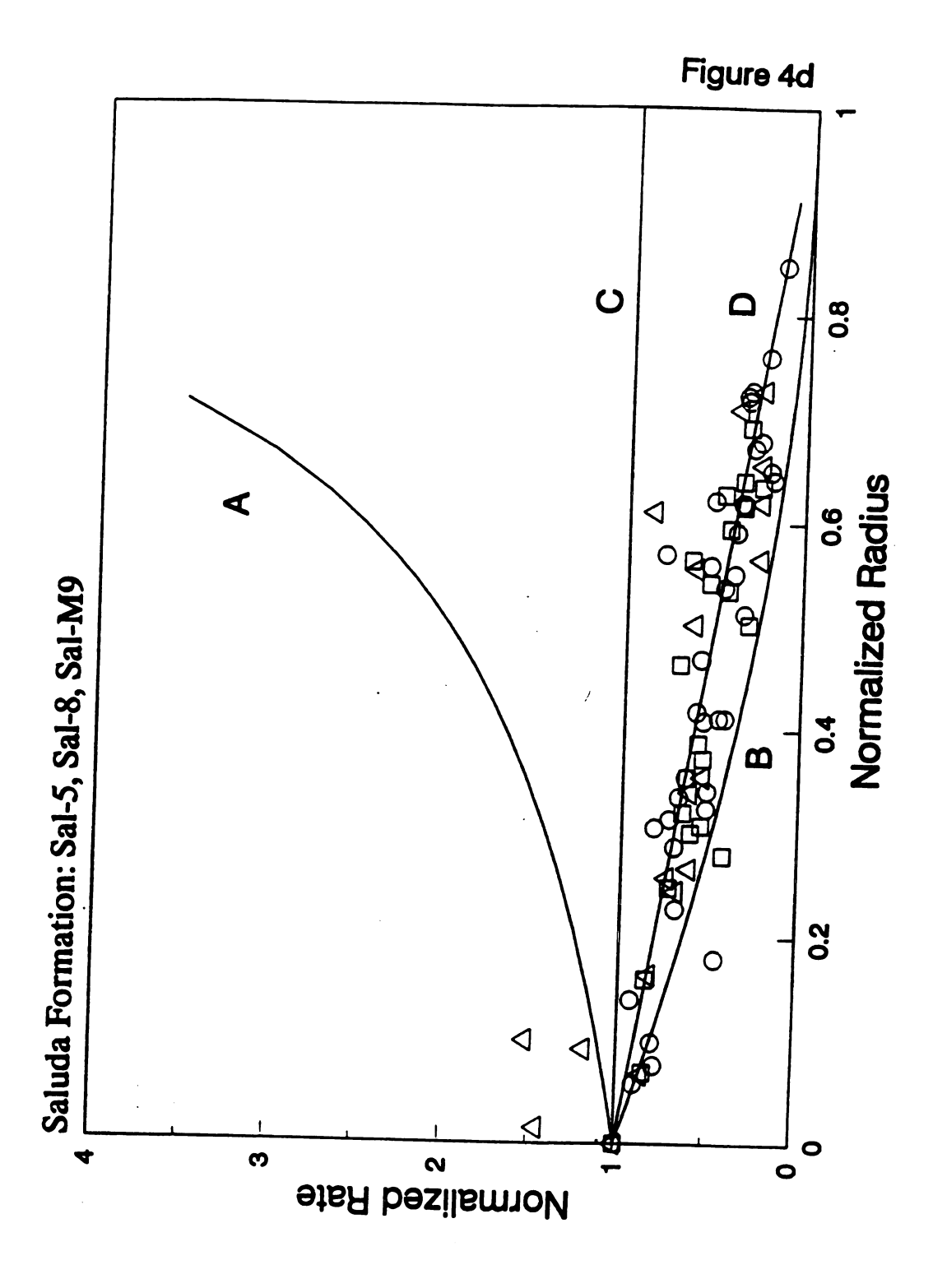
- a) Burlington-Keokuk Formation (Mississippian) from the Biggsville quarry. Sample BV-23, BV-25, and BV-4 are designated by open triangles, open squares, and filled squares respectively.
- b) Burlington-Keokuk Formation (Mississippian) from the Harper quarry. Samples HS-1, H-2, H-3, and H-4 are designated by asterisks, squares, triangles and circles respectively.
- c) Sero-Domi Formation (Pliocene) from Bonaire.

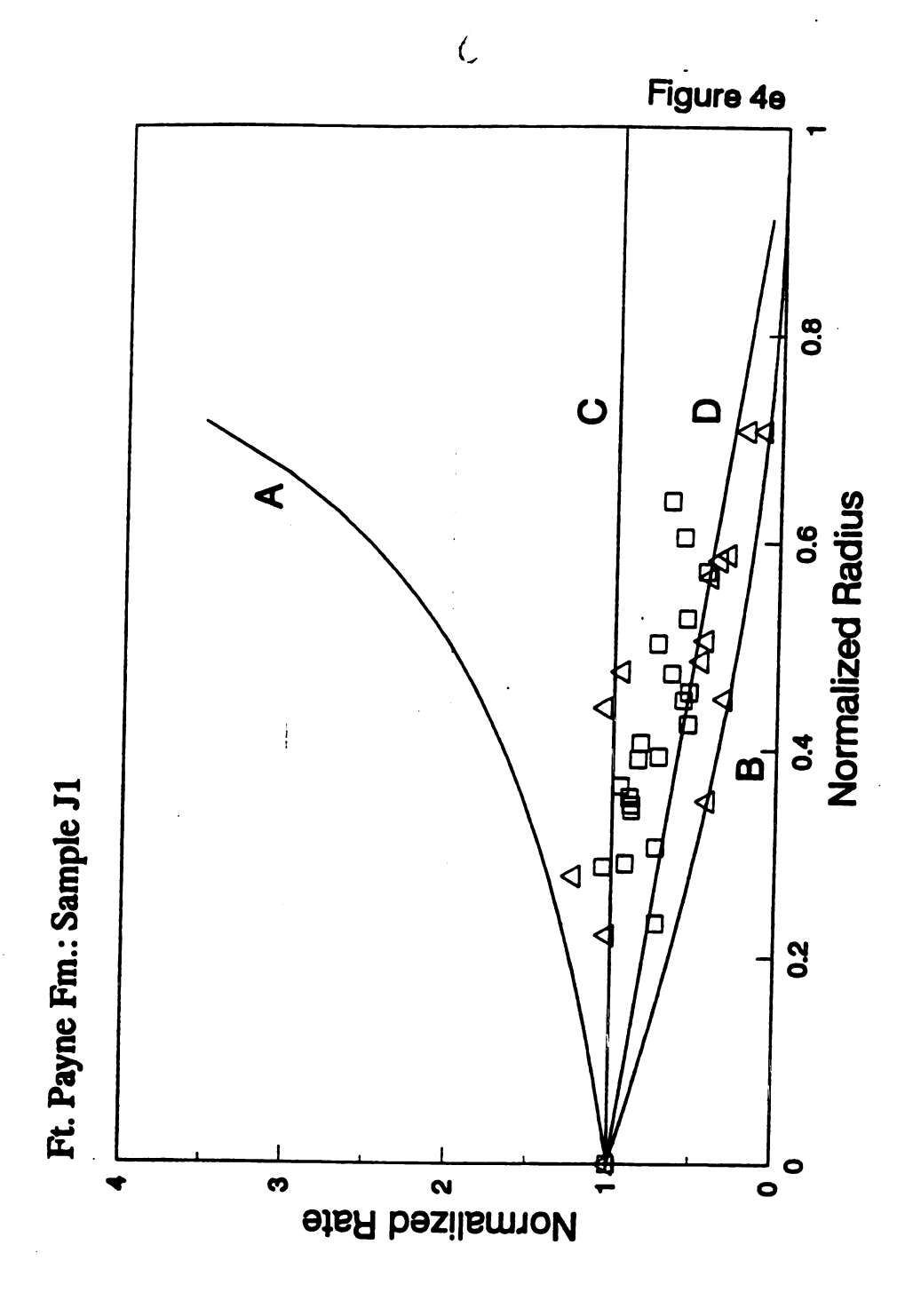
  Samples SC 34 E, SC 34 D, and SC 39 D are designated by squares, triangles and circles respectively.
- d) Ft. Payne Formation (Mississippian) from Jellico, Tennessee. The data are from two thin-sections cut from a single sample collected near the base of the unit.
- e) Saluda Formation (Ordovician) from near Madison,
  Indiana. Samples Sal-5, Sal-8 and M-9 are designated
  by squares, triangles and circles respectively.











## Discussion

The data suggest that one or two mechanisms may be responsible for the zonation patterns found in the dolomites used in this study. However, these relatively simple growth patterns may be explained in several ways.

Growth of Homogeneous Crystals from Homogeneous Solutions

Possible growth mechanisms may be constrained when crystal growth is assumed to occur in compositionally homogeneous solutions and involves constant crystal chemistry. These are the conditions for which the crystal growth laws in Table 1 were derived. Of the rate laws contained in Table 1, only surface-reaction-limited mechanisms can be used to explain these data. The data lie along a more or less linear trend that falls between the line for polynuclear or screw-dislocation-limited growth and the line for mononuclear surface-reaction-limited growth. A continuum of possible rate laws exists between the two endmember conditions of rapid nucleation with slow layer growth (polynuclear) and slow nucleation with rapid layer growth (mononuclear). The data trending along a line between these two endmembers may result from surfacereaction-limited conditions in which surface nucleation rates and layer growth rates are comparable. If this is so, then bulk dolomitization rates must also be sufficiently

slow so that solution compositions remain spatially constant.

Size Dependent Growth from Homogeneous Solutions

The observed growth rates may also be interpreted as being due to size dependent reaction rates operating under the conditions of spatially homogeneous solutions. If the crystal's surface composition changes as a function of it's size then the actual rate-limiting step will be masked by an apparent rate law that reflects the evolution in surface chemistry. Assuming that crystal growth is surface-reaction-limited and that the change in surface composition produces a linear dependence of the growth rate coefficient on crystal radius then a growth rate law may be derived as follows:

Eq. 15 dr/dt = k'r

where

k'r = k in case Ib or Ic of Table 1

All of the dolomites studied are calcium rich. This suggests that the crystal growth rate coefficient may not be constant throughout the growth history of a crystal. This would be especially significant when the core of a crystal is more calcian than is its rim because, as dolomite becomes less calcian, its solubility decreases (Carpenter 1980).

Therefore, the growth rate coefficient may be expected to increase as the crystal grows because the free energy difference between the reactive surface and the solution also increases (Nielsen 1964). This may be accomplished by forming nucleii of some constant calcium-rich composition and then epitaxially precipitate progressively less soluble material. This behavior has been observed in experiments in which dolomite grows by epitaxially precipitating material with progressively less calcium before achieving an ideal dolomite composition. Reeder and Prosky (1986) and Fouke and Reeder (1992) found sector zoned dolomite in the Burlington-Keokuk and Seroe Domi Formations in which calcium poor crystal faces grew faster than unequivalent crystal faces containing more calcium. It may therefore be argued that as the crystal grows by the addition of less calcium rich material the reaction rate increases because of an increased thermodynamic drive caused by increased disequilibrium between the crystal surface and solution. Ultimately, the surface composition may become that of ideal dolomite in which case the degree of disequilibrium achieves a maximum, constant value that is reflected in further growth by constant surface-reaction rates conforming to the surface-reaction-limited rate law in case Ib or Ic of Table The crystal zonation data in this study are consistent with a growth rate model in which the rate "constant" increases as the crystal grows.

Crystal Growth from Compositionally Inhomogeneous Solutions

Another explanation for the radius-rate data may be obtained when crystal growth does not involve spatially homogeneous solutions. Spatial inhomogeneity in solution composition could significantly influence crystal growth rates irrespective of the rate-limiting step governing individual crystal growth. This is because crystals growing from different solutions may be expected to grow at different rates. Crystal growth could still involve surface-reaction or diffusion-limited growth but these influences could be of secondary importance when compared to the potential variation in the magnitude of the saturation state. Therefore, crystal growth may no longer be a simple function of the rate-limiting step, but instead reflect spatial variation in solution composition.

If we assume that dolomite crystal growth kinetics are of the form found for calcite and aragonite precipitation, we may find a radius-rate relationship that explains these data. Calcite precipitation kinetics, when limited by surface-reaction rates, is consistent with the following empirical equation:

Eq. 16 
$$R = k \lambda (\Omega - 1)^n$$

where the precipitation rate (R in moles/ area-time) is a function of a reaction rate constant (k), reactive surface

area (A) and the degree of disequilibrium  $(\Omega-1)$  raised to the power of the reaction order (n). This may be rewritten in terms of crystal growth rate:

Eq. 17 
$$dV/dt = v k \lambda (\Omega-1)^n$$

where dV/dt is the volumetric crystal growth rate, and v is the molar volume. This may also be written in terms of radial growth rate (dr/dt):

Eq. 18 
$$dr/dt = v b k (\Omega-1)^n$$

where b is the geometric constant. If the growth rate and other parameters for the largest crystal are designated with primes then the normalized growth rate becomes:

Eq. 19 
$$\frac{dr/dt}{dr'/dt'} = \frac{k (\Omega-1)^n}{k' (\Omega'-1)^{n'}}$$

Integrating Eq. 19 from t=0 to t=t gives the crystal radius at time t. Designating the parameters of the largest crystal with primes and taking the ratio of the two radii gives the expression for the normalized radius:

Eq. 20 
$$\frac{\mathbf{r}}{\mathbf{r}'} = \frac{\mathbf{k} (\Omega - 1)^{\mathbf{n}} \mathbf{t}}{\mathbf{k}' (\Omega' - 1)^{\mathbf{n}'} \mathbf{t}'}$$

When precipitation is from compositionally homogeneous solutions, the primed rate constant, saturation state, and reaction order are equal to their unprimed counterparts so that the RHS of Eq. 19 is equal to one and the RHS of Eq. 13 reduces to the ratio of t to t'. This is the normalized radius-rate relationship for Case Ib or Ic of Table 1 and Curve C of Fig. 3. However, when two crystals grow from compositionally distinct solutions, then the primed and unprimed variables will not be equal. In this situation, the normalized radius will equal the normalized rate when nucleation is simultaneous (t=t'). This relationship follows line D in Fig. 3 and is consistent with the data in this study.

There are several factors in Eq. 19 or Eq. 20 that could be influenced by variations in solution composition. In Mg-calcite precipitation, reaction rates increase with supersaturation as a power function of the reaction order and as a linear function of the reaction rate constant (Morse 1983). In addition, other dissolved species such as orthophosphate, sulfate and the Mg/Ca ratio of the solution have also been found to change the rate constant and/or reaction order (Mucci and Morse 1983; Mucci 1986; Mucci et al. 1989). If, after simultaneous nucleation, dolomite behaves in a similar fashion, then the simple radius-rate relationship could result from a wide range of solute-induced variations in reaction kinetics caused by

solutions with spatially variable degrees of supersaturation.

In order to apply this model, the data must be reconciled to a situation in which dolomite nucleation is simultaneous and growth involves inhomogeneous solutions. The question of simultaneous nucleation may be explained by noting that the criteria used for crystal measurements require that an internal zone be present. Typically, this interior zone was significantly smaller than the zone measured. Therefore, measurements were made only on crystals that had all nucleated within the interval represented by the internal zone. Furthermore, differences in the time of nucleation within this interval could be expected to produce variation in the normalized radius (r/r') and the observed scatter of data about line D.

One way in which inhomogeneous solutions may be formed and maintained is by crystal growth induced depletion of solute during transport. The interaction of transport rates and reaction rates is commonly modeled using the advection-dispersion-reaction equation (Eq. 21) (Berner 1971; Palciauskas and Domenico 1976; Freeze and Cherry 1979; Berner 1980; Phillips 1991 and many others). Palciauskas and Domenico (1976) demonstrated that this equation, when adapted for dispersion free, one-dimensional flow with a first order reaction involving a single reactant, could be applied to carbonate systems. Under these conditions the

transport equation with reaction may be written as (Eq. 14, Palciauskas and Domenico 1976):

Eq. 21 
$$V \delta C/\delta x - D \delta^2 C/\delta x^2 = -k C$$

where C is the reactant concentration and x is the distance from recharge along the flowpath. Advective transport is controlled by the average linear fluid velocity (V) and diffusional transport is controlled by the diffusion coefficient (D). The reaction rate coefficient (k) is a function of the specific surface area and is defined as the ratio of the reactive surface area to pore volume. This approach allows for treating nonhomogeneous reactions as if they are homogeneous and continuous. Furthermore, the dependence of reaction rate on specific surface area allows for a wide range of bulk reaction rates controlled by the texture of the reacting sediment. For simplicity, the specific surface area, unless otherwise specified, will be assumed to be constant. In this approach, the change in solute concentration with time is equal to the difference in the rate reactants are supplied and removed by advection, hydraulic dispersion, and reactions.

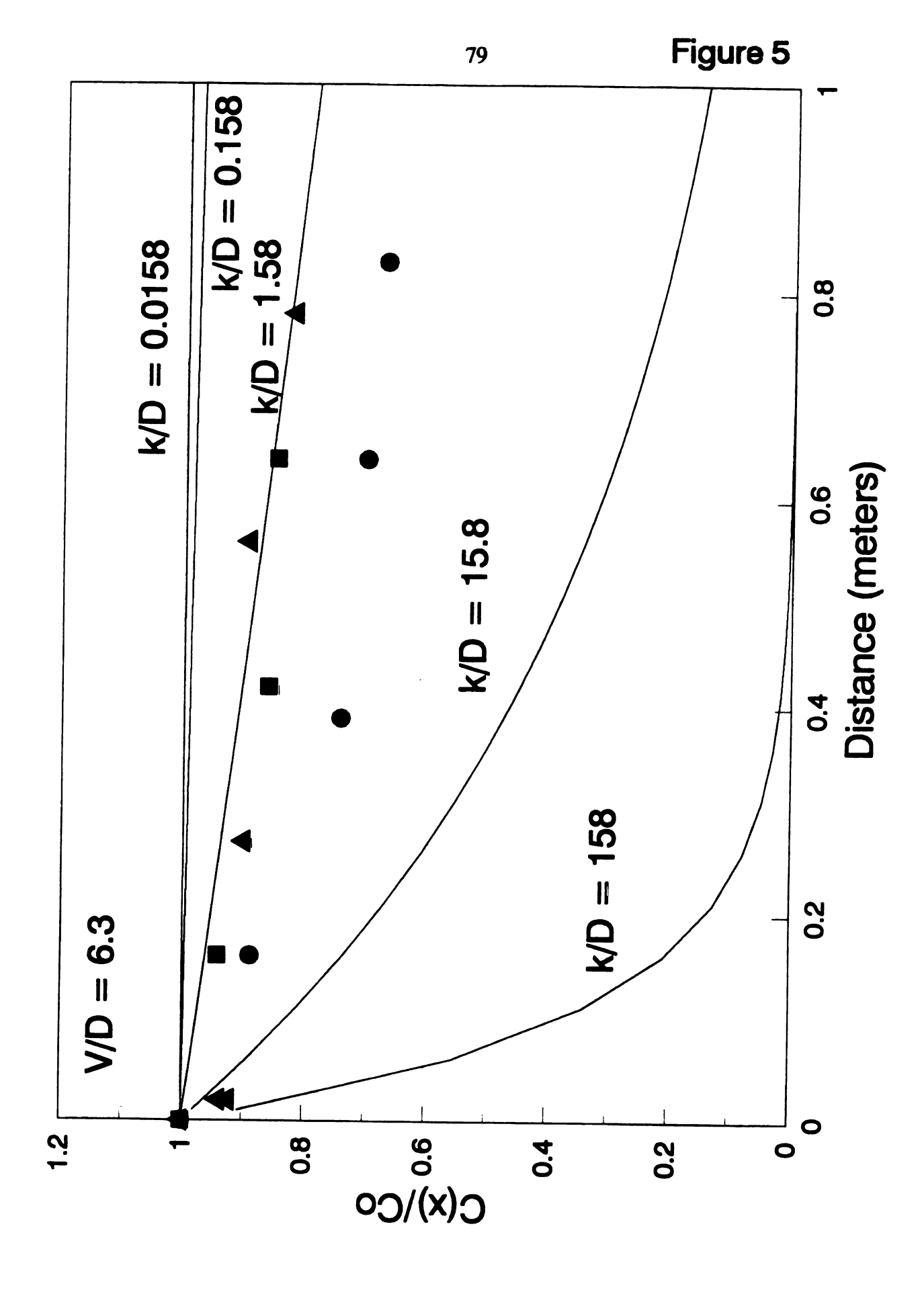
To illustrate the possibility of mixed transport and reaction-limited growth in the formation of dolomite, Eq. 21 was applied to the concentration gradients found by Patterson and Kinsman (1982) in three vertical sequences of

pore waters associated with active dolomitization in a sabka near Abu Dhabi. If magnesium is assumed to be the single reactant whose concentration controls the saturation state of the solution, then Eq. 21 should provide insight concerning the interaction of reaction rates and transport rates. Palciauskas and Domenico, (1976) provide a solution to Eq. 21 when a reactant enters the sediment at a rate just equal to the rate it is transported into the matrix by advection and dispersion, and when the change in reactant concentration with distance eventually disappears. When these conditions are met, the distance into the porous media (X) over which the reactant concentration at the interface between a homogeneous source solution and the porous media (C<sub>O</sub>) is reduced to C(x) is given by (see Eq. 25, Palciauskas and Domenico 1976):

Eq. 22 
$$X = \frac{2}{V/D(1-(1+4 kD/V^2)^{1/2})} \ln \frac{C(x)}{C_0}$$

where fluid velocity (V), dispersion coefficient (D), and the reaction rate (k) all interact to control the solution composition during reactant transport.  $C_0$  and C(x) are the reactants concentration in excess of the equilibrium concentration of  $Mg^{2+}$  in which dolomite saturation is buffered by aragonite. Figure 5 illustrates the relationship between the expected concentration gradient and various reaction rates relative to the diffusion coefficient of  $Mg^{2+}$  in water. This plot uses Patterson and Kinsman's

Figure 5 Theoretical Mg<sup>2+</sup> concentration gradients from Eq. 22 for various reaction rates (k). All of the curves assume a flow velocity (V) of 0.4 m/yr and a diffusion coefficient (D) for Mg<sup>2+</sup> of 2 X 10<sup>-9</sup> m<sup>2</sup>/sec. The curves are designated by the ratio of the bulk reaction rate to the diffusion coefficient (k/D). The symbols are data from pore fluid collected by Patterson and Kinsman (1982) from their cores CA'1 (triangles), CC'1 (circles), and CC'4 (squares). These data were normalized to dolomite saturation in an aragonite buffered system. This was done by subtracting the Mg2+ concentration of the pore water from the equilibrium concentration as specified by Palciauskas and Domenico (1976).



(1982) downwardly directed flow velocity of 0.4 m/yr and a Mg<sup>2+</sup> diffusion coefficient of 2 X 10<sup>-9</sup> m<sup>2</sup>/sec. This diffusion coefficient is probably an extremely high value, considering that diffusion coefficients decrease significantly in sediments (Freeze and Cherry 1979; Berner 1980). In this diagram, the Mg<sup>2+</sup> gradient from Patterson and Kinsman's (1982) study indicates that the minimum bulk dolomitization rate is about the same as the diffusion coefficient of Mg<sup>2+</sup> in seawater. Decreasing the diffusion coefficient to a more "real" value typical of sediments would simply increase the required bulk reaction rate by an equivalent factor. This result, seems to indicate that modern dolomite growth rates may be sufficiently rapid to deplete a dolomitizing fluid of Mg<sup>2+</sup> as it flows through an aragonite rich sediment.

Calcium and magnesium concentration gradients in pore waters associated with modern dolomite in sediments from Kau Bay are consistent with a model in which bulk reaction rates are approximately equal to diffusion. Middelburg et al. (1990) found Ca<sup>2+</sup> and Mg<sup>2+</sup> gradients extending from the sea floor to the top of a dolomite rich layer at a depth of about 350 cm. Supersaturations with respect to calcite and dolomite are roughly constant for the first 200 cms depth and then decrease almost an order of magnitude with respect to dolomite in the meter or so of sediment overlying the dolomite layer.

Observations from ancient dolomites are also consistent with spacially inhomogeneous solutions. In the Burlington-Keokuk Formation, Choquette et al. (1991), describe the heterogeneous distribution of a luminescent zone that marks the end of the first episode of dolomitization. This luminescent zone was found on crystal faces lining pores but was absent on the faces in contact with the matrix. This observation of heterogeneity in the distribution of a luminescent zone seems to contradict the assumption of crystal growth from spatially homogeneous solutions. This also suggests that the last stage of this dolomite's growth may have been restricted to advectively supplied pores in which reactions forming the final luminescent zone occurred at a high enough rate to prevent solute migration into the matrix.

The sector zoning chemistry (Reeder and Prosky 1986; Fouke and Reeder 1992), the observation of textural controls on the distribution of luminescent zonation (Choquette et al. 1991), and the results of this study are consistent with surface-reaction-limited growth that induces and maintains heterogeneous solutions that result in crystal growth involving spatially varying reaction kinetics.

# Conclusions

We have found in the cathodoluminescent zonation of dolomite, formed under near surface conditions, a coherent pattern of crystal growth in which small crystals grow slower than large crystals. This pattern is apparently unconstrained with respect to location or time and may reflect processes common to a wide range of low-temperature dolomites. The zonation pattern may be reconciled to several possible crystal growth mechanisms upon the imposition of various constraints. Under the assumption of spatial homogeneity of solution composition and continuous nucleation, these data are consistent with surface-reactionlimited kinetics involving growth through a 2-D nucleation and spread model or one in which there are systematic changes in the surface composition of the growing crystal. In order to satisfy this assumption, individual crystal growth rates as well as the bulk rate of sediment dolomitization must be much less than reactant transport rates.

These data are also consistent with instantaneous nucleation followed by crystal growth from solutions whose composition is spatially inhomogeneous. Under this assumption, the pattern of growth may reflect a situation in which bulk dolomitization rates are about the same as the rate of reactant supply. This implies that whatever the

mechanism by which dolomite grows, it is not much slower than the rate of solute transport by diffusion and could be somewhat greater.

# **BIBLIOGRAPHY PART II**

#### References

- Baker, P.A. and Burns, S.J., 1985, Occurrence and Formation of Dolomite in Organic-Rich Continental Margin Sediments, The American Association of Petroleum Geologists Bulletin, v 69, p 1917-1930.
- Baker, P.A. and Kastner, M., 1981, Constraints on the formation of sedimentary dolomite, Science, v. 213, p. 214-216.
- Banner, J.L., Hanson, G.N. and Meyers, W.J., 1988, Water-Rock Interaction History of Regionally Extensive Dolomites of the Burlington-Keokuk Formation (Mississippian): Isotopic Evidence, in Shukla and Baker (ed.) Sedimentology and Geochemistry of Dolostones, SEPM Special Publication No. 43, p. 97-113.
- Banner, J.L., Hanson, G.N. and Meyers, W.J., 1988a,
  Determination of initial Sr isotopic compositions of
  dolostones from the Burlington-Keokuk formation
  (Mississippian): Constraints from cathodoluminescence,
  glauconite paragenesis and analytical methods. Jour.
  Sed. Petrology, V 58, p 673-687.
- BeMent, W.O., Elias, R.J., Goodman, W.R., Bacon, R., Yu, H.S., Potter, P.E., 1981, Mississippian and Pennsylvanian section on Interstate 75 south of Jellico, Campbell County, Tennessee, Report of Investigations, Division of Geology, V 38, 42p.
- Berner, R.A., 1971, Principles of Chemical Sedimentology, McGraw-Hill, New York, 240 p.
- Berner, R.A., 1980, Early Diagenesis; A Theoretical Approach, Princeton University Press, Princeton, N.J. 241 p.
- Brown, C.D. jr., and L.A. Lineback, 1966, Lithostratigraphy of Cincinnatian Series (Upper Ordovician) in Southwestern Indiana. A.A.P.G., V. 50, p 1018-1032.
- Burton, W.K., Cabrera, N. and Frank, F.C., 1951, The growth of crystals and the equilibrium structure of their surfaces, Phil. Trans. Royal Soc. London, A234, p 299-358.
- Butler, G., 1969, Modern evaporite deposition and geochemistry of coexisting brines, the Sabkha, Trucial Coast, Arabian Gulf, Journal of Sedimentary Petrology, V. 39, p. 70-89.

- Cander, H.S., Kaufman, J., Daniels, L.D., and Meyers, W.J., 1988, Regional Dolomitization of Shelf Carbonates in the Burlington-Keokuk (Mississippian), Illinois and Missouri: Constraints from Cathodoluminescent Zonal Stratigraphy, in Shukla and Baker (ed.), Sedimentology and Geochemistry of Dolostones, SEPM Special Publication No. 43, p. 129-144.
- Carlson, M.P. 1979, The Nebraska-Iowa Region, in Craig, L.C. and Varnes, K.L., eds., Paleotectonic Investigations of the Mississippian System in the United States, Part I: Introduction and Analyses of the Mississippian System: U.S. Geological Survey Professional Paper No 1010-F, p 107-114.
- Carlson, W.D., 1989, The significance of intergranular diffusion to the mechanisms and kinetics of porphyroblast crystallization., Contributions to Mineralogy and Petrology, V 103, p. 1-24.
- Carpenter, A.B., 1980, The chemistry of dolomite formation I: the stability of dolomite, in Zenger, Dunham and Ethington (ed.) Concepts and Models of Dolomitization, SEPM Special Pub. No. 28, p 111-121,
- Choquette, P.W., Cox, A., Meyers, W.J., 1991, Characteristics, distribution and origin of porosity in shelf dolostones: Burlington-Keokuk Formation (Mississippian), U.S. mid-continent.
- Chowns, T.M., Elkins, J.E., 1974, The origin of quartz geodes and cauliflower cherts through the silicification of anhydrite nodules, Journal of Sedimentary Petrology, V 44, p 885-903.
- Compton, J.S., 1988, Degree of supersaturation and precipitation of organogenic dolomite, Geology, v 16, p 318-321.
- De Buisonje, P.H., 1974, Neogene and Quaternary Geology of Aruba, Curacao and Bonaire, Martinus Nijhoff, The Hague 291 p.
- Fouke, B.W., Reeder, R.J., 1992, Surface structural controls on dolomite composition, evidence from sector zoning, Geochim et Cosmochim. Act., V 56, p 4015-4024.
- Freeze, R.A., Cherry, J.A., Groundwater, Prentice-Hall, Englewood Cliffs, New Jersey, 604 p.
- Hatfield, C.B., 1968, Stratigraphy and Paleoecology of the Saluda Formation (Cincinnatian) in Indiana, Ohio Kentucky., G.S.A. Special Paper 95.

- Lucia, F.J., Major R.P., in prep
- Kaufman, J., Cander, H.S., Daniels, L.D., Meyers, W.J., 1988, Calcite cement stratigraphy and cementation history of the Burlington-Keokuk Formation (Mississippian), Illinois and Missouri. Jour. Sed. Petrology, V 58, p 312-326.
- Kretz, R., 1974, Some models for the rate of crystallization of garnet in metamorphic rocks., Lithos, Vol. 7, p. 123-131.
- Machel, H.G. and Mountjoy, E.W., 1986, Chemistry and Environments of Dolomitization - A Reappraisal, Earth-Science Reviews, V 23, p 175-222.
- Martin, W.D., 1975, Petrology of Cincinattian Series Limestones. Journal of Sedimentary Petrology, V.45, p. 907-925.
- Mazzulo, S.J., Reid, A.M., Gregg, J.M., 1987, Dolomitization of Holocene Mg-calcite supratidal deposits, Ambergris Cay, Belize, Geological Society of America, v 98, p 224-231.
- Middelburg, J.J., de Lange, G.j., Kreulen, R., 1990, Dolomite formation in anoxic sediments of Kau Bay, Indonesia, Geology, v 18, p. 399-402.
- Morse, J.W., 1983, The Kinetics of calcium carbonate dissolution and precipitation, in Reeder R.J. (ed.), Carbonates: Mineralogy and Chemistry, Mineralogical Society of America, p 277-264.
- Mucci A., 1986, Growth kinetics and composition of magnesium calcite overgrowths precipitated from seawater: quantitative influence of orthophosphate ions, Geochim et Cosmochim Acta, V 50, p 2255-2265.
- Mucci A., Canuel, R., Zhong, S., 1989, The solubility of calcite and aragonite in sulfate-free seawater and the seeded growth kinetics and composition of the precipitates at 25°C, Chemical Geology, V 74, p 309-320.
- Mucci A., Morse, J.W., 1983, The incorporation of  $Mg^{2+}$  and  $Sr^{2+}$  into calcite overgrowths: influences of growth rate and solution composition, Geochim et Cosmochim, V 47, p 217-233.
- Nielsen, A.E., 1964, Kinetics of precipitation, Macmillan, New York, 151 p.

- Ohara, M, Reid, R.C., 1973, Modeling Crystal Growth Rates from Solution, Prentice-Hall, Englewood cliffs, N.J., 272 p.
- Patterson, R.J., Kinsman, D.J.J., 1982, Formation of diagenetic dolomite in coastal sabka along Arabian (Persian) Gulf. A.A.P.G. V66, p 28-43.
- Palciauskas, V.V., Domenico, P.A., 1976, Solution chemistry, mass transfer, and the approach to chemical equilibrium in porous carbonate rocks. Geol. Soc. of Amer. Bull., V 87, p 207-214.
- Pierre, C., Ortlieb, L., Person, A., 1984, Supratidal Evaporitic Dolomite at Ojo De Liebre Lagoon: Mineralogical and Isotopic Arguments for Primary Crystallization, Journal of Sedimentary Petrology, V. 54, p. 1049-1061.
- Pingatore, N.E. jr., 1976, Vadose and Phreatic Diagenesis: Processes Products and Their Recognition in Coral, Journal Sedimentary Petrology, v 46 p 985-1006.
- Phillips, O.M. 1991, Flow and Reactions in Permeable Rocks, Cambridge University Press, Cambridge, U.K., 285 p.
- Reeder, R.J., Prosky, J.L., 1986, Compositional sector zoning in dolomite, Jour. Sed. Petrology, V 56, p 237-247.
- Sibley, D.F., 1980, Climatic Control of Dolomitization, Seroe Domi Formation (Pliocene), Bonaire, N.A., in Zenger, Dunham and Ethington (ed.), Concepts and Models of Dolomitization, SEPM Special Pub. No. 28, p. 247-258.
- Staudt, W.J., Oswald, E.J., and Schoonen, M.A.A., 1993, Determination of sodium, chloride, and sulfate in dolomites: a new technique to constrain the composition of dolomitizing solutions: Chem. Geol. 107, 97-109.
- Warren, J.K., 1990, Sedimentology and mineralogy of dolomitic Coorong lakes, South Australia, Journal of Sedimentary Petrology, v 60, p 843-858.

# APPENDIX I

Table Al.1
Reactant Data

# Isothermal Baseline

Sample	Date-Bomb	Calcite Wt. (g)	Wt Sol'n (g)	Wt Loss (g)
I-1	3-17-91-a	0.0996	16.0231	0.4015
I-2	3-19-91-d	0.1001	16.0576	0.3998
<b>I-3</b>	3-22-91-a	0.0997	16.0348	0.4145
I-4	3-23-91-b	0.1001	16.0811	0.3486
I <b>-</b> 5	3-23-91-c	0.1002	16.0764	0.5100
I <b>-</b> 6	3-23-91-d	0.0996	16.0835	0.2742
I-7	4-1-91-a	0.1000	16.1285	0.4369
I-8	4-2-91-b	0.1001	16.1202	0.4498
I-9	4-1-91-c	0.0998	16.0308	0.4537
I-10	4-1-91-d	0.1002	16.0584	0.3641
I-11	4-6-91-a	0.1001	16.1122	0.5031
I-12	4-11-91-a	0.1002	15.8287	0.5160

12 Hour Cycled

Sample	Date-Bomb	Calcite Wt. (g)	Wt Sol'n (g)	Wt Loss (g)
12-1	4-12-91-c	0.1002	16.0545	0.2962
12-2	4-11-91-d	0.1000	16.1330	0.2913
12-3	5-8-91-d	0.1001	16.1529	0.3641
12-4	5-8-91-c	0.1002	16.0725	0.4199
12-5	5-8-91-b	0.1000	16.0902	0.4102
12-6	5-27-91-a	0.1002	16.1185	0.5192
12-7	5-23-91-d	0.1005	16.1406	0.3528
12-8	2-5-92-a	0.1001	16.1363	0.2775
12-9	2-6-92-b	0.1002	16.1087	0.2236
12-10	2-8-92-c	0.0999	16.1033	0.1337
12-11	2-10-92-d	0.1001	16.1147	0.3261

Table A1.1 (Cont.)

# 48 Hour Cycled

Sample	Date-Bomb	Calcite Wt. (g)	Wt Sol'n (g)	Wt Loss (g)
48-1	6-3-91-a	0.0999	16.0315	0.2749
48-2	6-3-91-b	0.1000	16.0684	0.4901
48-3	6-3-91-d	0.1001	16.0680	0.2897
48-4	12-3-91-b	0.1002	16.1385	0.4232
48-5	12-3-91-c	0.0998	16.0483	0.2636
48-6	12-10-91-a	0.1000	16.1256	0.1384
48-7	12-11-91-b	0.0950	16.1051	0.2647
48-8	1-7-92-a	0.1001	16.1564	0.1726
48-9	1-7-92-b	0.1000	16.2189	0.1437
48-10	1-7-92-c	0.1002	16.1435	0.1633
48-11	1-8-92-d	0.1003	16.2515	0.1809

Table A1.2

XRD Data

Cu ka, 25 ma, 35 kV, 0.5° 20 per min

Isothermal

Sample		Peak Position	ition	ပိ	Correction	Corre	Corrected Position	ition
•	Fluorite	rite Calc.	HIMC	D01.		Calc.	HMC	Dol.
I-1	•	29.47	!	1	00.0	29.47	1 1 1	!
I-2	•	1	!!!!!!!!!!!!!!!!!!!!!!!!!!!!!!!!!!!!!!!	31.05	-0.10	1	1	30.95
I-3	•	29.50		!	-0.10	29.40		!!!!!!!!!!!!!!!!!!!!!!!!!!!!!!!!!!!!!!!
I-4	•	29.51	30.66	1	-0.10	29.41	30.56	!!!!
I-5	•	!!!!!!!!!!!!!!!!!!!!!!!!!!!!!!!!!!!!!!!	1 1	31.05	-0.07	1 1	1	30.98
9 <b>-</b> I	•	1	!!!!!!!!!!!!!!!!!!!!!!!!!!!!!!!!!!!!!!!	31.05	-0.03	1 1	1 1	31.02
Ĺ	•	29.53	!!!	!!!	-0.09	29.44	1	!!!
I-8	•	!!!	!!!!	31.00	-0.11	 	1	30.89
6-I	28.39	29.50	30.71	31.01	-0.09	29.41	30.62	30.92
1-10	•	29.55	!!!!	!!!	-0.13	29.42	!	!!!
I-11	•	29.52	30.71	!!!!!!!!!!!!!!!!!!!!!!!!!!!!!!!!!!!!!!!	-0.15		•	1
I-12	•	29.38	30.55	!	0.04	29.42	30.59	!!!!

Table A1.2 (cont.) 12 Hour Cycled

ition	Dol.			1			1	1	30.83	30.87	30.95	!
Corrected Position	НМС	30.63	30.66	30.59	30.59	30.56	30.57	30.60	30.61	30.59	1	30.54
Corre	Calc.	4	4	4	29.45	4	4	4	4	3	1	29.41
Correction		-0.06	-0.01	-0.11	-0.07	-0.10	-0.07	-0.10	-0.10	-0.15	-0.15	-0.17
S S	Dol.	 	1		1	1 1	1	!!!!!!!!!!!!!!!!!!!!!!!!!!!!!!!!!!!!!!!	30.93	31.02	_	
ition	HMC				30.66						!!!	30.71
Peak Position	te Calc.	29.51	29.49		29.52			29.56	29.51	29.51	1	29.58
	Fluorite	۳.	٠,	4.	28.37	4.	<b>.</b>	4.	4.	4.	4.	4
Sample	ı	2	12-2	2	12-4	12-5	2	2	2	2	12-10	12-11

Table Al.2 (cont.)

48 Hour Cycled

Sample		Peak Position	ition	ပိ	Correction	Corre	Corrected Position	ition
	Fluorite	Calc.	HMC	Dol.		Calc.	HMC	Dol.
48-1	۲	רא סכ	•			<b>I</b> ₹	70 60	
1	. 4	29.56	30.62	30.97		29.46	30.52	30,87
1		29.50		• 1		29.44	1   0   •   0	• • •
48-4	28.39	29.54	30.70	31.00	60.0-	29.45	30.61	30.91
- 1	<u>ب</u>	29.46	30.70	30.95		29.40	30.64	30.89
•	4	29.54	30.72	31.01		29.38	30.56	30.85
1		29.53	30.72	31.01		29.45	30.64	30.93
•	4.	!	1	31.06		!	!!!!!!!!!!!!!!!!!!!!!!!!!!!!!!!!!!!!!!!	30.96
48-9	4	29.55	30.67	!		29.43	30.55	!!!!!!!!!!!!!!!!!!!!!!!!!!!!!!!!!!!!!!!
48-10	ທ	!!!	!	1.			!	•
48-11	28.36	1	!	31.00	-0.06	1	1	30.94

Table Al.3

Peak Height and Product Proportion Data Fluorite Standard

Isothermal

Calcite	ite 0	HWC			•	rercent		Time
I-1 100.	00	c	Dol.	Calc.	HIMC	Dol	Prod.	(hrs)
	0	>	0.0	100.	0.	0.	0.	99.75
I-2 0.		0.0	100.0	•	•	100.	100.	144.00
I-3 100.	0	0.0	0.0	100.	•	•	•	92.50
I-4 26.		6.7	0.0	80.	20.	•	20.	114.25
I-5 0.		0.0	100.0	•	•	100.	100.	119.50
I-6 0.0		0.0	100.0	•	•	100.	100.	126.25
I-7 100.		0.0	0.0	100.	•	•	•	100.30
		0.0	100.0	•	•	100.	100.	•
		3.9	22.1	•	36.	58.	94.	•
I-10 100.		0.0	0.0	100.	•	•	•	•
		0.2	0.0	98.	2	•	2	105.63
I-12 26.		5.5	0.0	83.	17.	•	17.	108.20

Table Al.3 (cont)

12 Hour Cycled

Sample	Peal	<b>Peak</b> Height	ht		Per	Percent		Heating Time
	Calcite	HMC	Dol.	Calc.	HMC	Dol	Prod.	(hrs)
12-1	18.7	9.0	0.0	96.	4.	0.	4.	109.90
12-2	28.8	4.0	0.0	88	12.	•	12.	107.10
12-3	19.4	0.7	0.0	97.		•		106.83
12-4	32.9	1.7	0.0	95.	<u>س</u>	•	ა.	108.60
12-5	12.8	1.5	0.0	.06	10.	•	10.	112.55
12-6	•	11.3	0.0	59.	41.	•	41.	168.62
12-7	σ.	1.8	0.0	93.	7.	•	7.	124.73
12-8	2.7	25.2	18.2	•	55.	39.	94.	180.67
12-9	7	23.4	31.9	4.	41.	55.	96	192.50
12-10	0.	0.0	100.0	•	•	100.	100.	216.50
12-11	4.4	13.8	0.0	24.	76.	•	.9/	24

Table Al.3 (cont)

48 Hour Cycled

Sample	Pea)	Peak Height	ht		Per	Percent		Heating
	Calcite	HMC	Dol.	Calc.	HMC	Dol	Prod.	(hrs)
48-1	10.9	10.8	0.0	50.	50.	0	50.	119.63
48-2	4.3	12.1	10.5	16.	45.	39.	84.	109.63
48-3	100.0	•	0.0	100.	•	•	•	110.80
48-4	32.0	5.6	4.0	83.	7.	10.	17.	15.
48-5	8.6	4.5	7.4	45.	21.	34.	55.	
48-6	4.8	14.0	25.0	11.	32.	57.	89.	120.50
48-7	15.6	19.5	14.3	32.	39.	29.	68.	
48-8	0.0	0.0	100.0	•	•	100.	100.	132.95
48-9	8.0	11.0	0.0	42.	58.	•	58.	137.70
48-10	0.0	0.0	100.0	•	•	100.	100.	144.23
48-11		0.0	100.0	•	•	100.	100.	155.77

### **APPENDIX II**

### Appendix A2

The data in this study were obtained by measuring the parameters in Fig A2.1 from photomicrographs of cathodoluminescent dolomite crystals recorded on 35 mm film. The measurements A, B, M1, M2, M3, and M4 were made using a reticle mounted in a binocular microscope. The raw measurements were converted to microns and are presented in Table A2.1

The processing of the data involved a geometric correction and a normalization procedure. The geometric correction involved rotating the rhomb about an axis extending between the acute interior angles of the apparent rhomb (See Fig A2.1). This was done using measurements A, B, and C. The cosines of angles B, and B were found as follows (See Fig. A2.2):

A2.1 Cos 
$$\beta = (\lambda^2 + \beta^2 - C^2)/2\lambda B$$

A2.2 Cos 
$$\theta = (B^2 + C^2 - A^2)/2BC$$

The altitude D of the triangle ABC was given by:

A2.3 D = 
$$[B^2+(C/2)^2-BC \cos \theta]^{1/2}$$

and the cosine of the angle  $\tau$  was found with:

A2.4 Cos 
$$\tau = (D^2 + (C/2)^2 - B^2)/DC$$

If the angle  $\tau$  was not within +/- 5° of 90° then the crystal measurement was not used. The expected crystal radius (T) associated with measurement D was found as follows:

A2.5 
$$T = D Tan 1/2 (73^{\circ} 15')$$

The ratio of the observed to the expected radius provides the required correction factor Cos F (See Fig. A2.2).

A2.6 
$$Cos F = C/2T$$

The corrected crystal diameters C' and E' are found as follows:

A2.7 
$$C' = C/\cos F$$

and

A2.8 
$$E' = E/\cos F$$

The corrected zone thickness (ZT) is given by:

A2.9 
$$ZT = (C'-E')/2$$

and the corrected crystal radius (CR) measured to the midpoint of the zone of interest is given by:

$$A2.10$$
 CR =  $(E'+ZT)/2$ 

The various radii (CR) were normalized to the largest crystal radius (CR\*) as follows:

and the various zone thicknesses were normalized to the corresponding zone thickeness ( $ZT^*$ ) of the largest crystal as follows:

Example using measurement #2 for sample BV-4

$$A = 12.00$$
  $B = 12.75$   $C = 13.50$   $E = 6.00$ 

Cos 
$$\beta = (A^2+B^2-C^2)/2AB = 0.406$$
  
Cos  $\theta = (B^2+C^2-A^2)/2BC = 0.5833$   
 $D = (B^2+(C/2)^2-BC \cos \theta)^{1/2} = 10.38$   
Cos  $\tau = (D^2+(C/2)^2-B^2)/DC = -.066$   
 $\tau = 93.8^{\circ}$   
 $T = D \text{ Tan } 1/2 (73^{\circ} 15') = 7.71$   
Cos  $F = C/2T = 0.8755$   
 $C' = C/\cos F = 15.42$   
 $E' = E/\cos F = 6.85$ 

$$ZT = (C'-E')/2 = 4.285$$

$$CR = (E'+ZT)/2 = 5.567$$

normalizing CR to the largest crystal radius (#19 where  $CR^* = 21.25$  and  $ZT^* = 14.89$ ) gives:

Normalized Radius =  $1-(CR/CR^*)$  = 0.738 Normalized Rate =  $ZT/ZT^*$  = 0.287

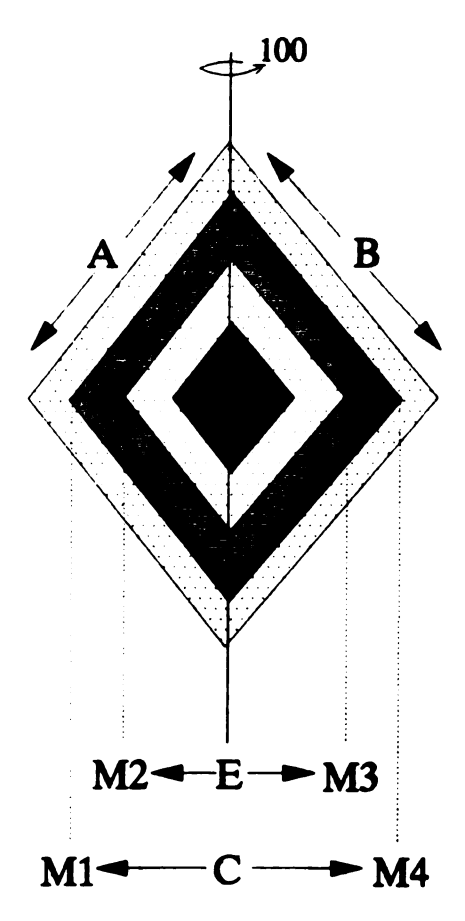


Figure A2.1 Schematic zoned dolomite showing side measurements A and B and radial measurements M1-M4 used to find radial measurements C and E.

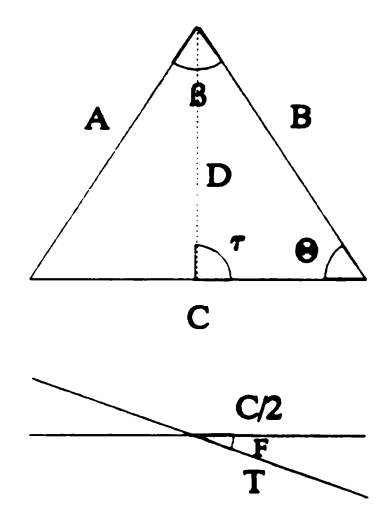


Figure A2.2 Triangle constructed from measurments in A2.1.

Table A2.1
Crystal Zonation Data

Sample BV-4

Meas	# A	В	С	E	Norm	alized
	microns	microns	microns	microns	radius	rate
2	12.00	12.75	13.50	6.00	0.73	0.29
3	47.25	45.00	54.75	24.75	0.03	1.01
4	25.50	27.00	25.50	12.00	0.41	0.60
5	19.50	20.25	22.50	11.25	0.58	0.41
6	34.88	34.88	40.50	15.75	0.24	0.86
7	15.75	15.75	18.00	9.00	0.67	0.32
8	20.25	21.38	22.50	11.25	0.55	0.43
9	16.88	18.00	22.50	12.38	0.62	0.34
10	13.50	13.50	16.88	10.13	0.72	0.22
11	46.13	47.25	50.63	28.13	0.02	0.86
12	20.25	21.38	23.63	11.25	0.56	0.44
14	27.00	27.00	31.50	13.50	0.42	0.62
15	19.13	19.13	22.50	12.38	0.61	0.34
16	28.13	28.13	33.75	15.75	0.41	0.60
17	30.38	30.38	36.00	20.25	0.39	0.53
18	34.88	34.88	42.75	16.88	0.23	0.86
19	47.25	47.25	54.00	25.88	0.00	1.00
20	23.63	24.75	27.00	13.50	0.49	0.50
25	13.50	13.50	14.63	7.88	0.71	0.26
26	14.63	14.63	15.75	6.75	0.68	0.35
27	11.25	11.25	14.63	5.63	0.74	0.30

Table A2.1

Sample BV-23

Meas	# A	В	С	E	Norm	alized
	microns	microns	microns	microns	radius	rate
-	10.00	10.75	15 00	10 50	0.72	0 22
1	12.00	12.75	15.00	10.50	0.73	0.22
2	20.25	19.50	23.25	12.75	0.54	0.53
3	11.25	11.25	12.75	6.75	0.73	0.32
4	12.00	12.75	15.00	11.25	0.74	0.19
5	40.50	42.75	51.00	38.25	0.10	0.63
6	24.00	23.25	26.25	17.25	0.46	0.49
9	22.50	24.00	27.00	15.00	0.46	0.62
10	26.25	26.25	29.25	17.25	0.39	0.66
11	22.50	22.50	22.50	12.00	0.44	0.67
12	12.00	12.75	15.00	9.75	0.72	0.26
13	42.00	43.50	45.75	28.50	0.00	1.00
14	12.00	11.25	15.00	7.50	0.71	0.37
16	18.00	19.50	24.00	16.50	0.57	0.37
17	33.00	33.75	41.25	20.25	0.19	1.04
18	16.50	15.75	17.25	11.25	0.63	0.35
19	26.25	25.50	30.00	15.75	0.39	0.74
20	22.50	24.00	31.50	18.75	0.41	0.63
21	15.00	15.75	18.75	12.75	0.66	0.30
22	18.00	17.25	18.00	10.50	0.57	0.46
24	13.50	14.25	15.00	11.25	0.69	0.21
25	23.25	24.00	31.50	17.25	0.39	0.70
26	22.50	23.25	26.25	17.25	0.49	0.47
27	15.75	15.00	16.50	11.25	0.65	0.30
29	12.00	12.00	14.25	9.75	0.74	0.22
31	21.75	22.50	24.75	18.00	0.51	0.37
32	25.50	26.25	33.75	18.75	0.35	0.74
33	18.75	18.00	21.00	12.00	0.57	0.47
34	21.75	21.75	24.00	15.00	0.50	0.50

Table A2.1

Sample BV-25

Meas	# A	В	С	E	Norm	alized
	microns	microns	microns	microns	radius	rate
1	15.00	15.00	15.00	10.50	0.63	0.30
2	15.75	15.75	18.00	11.25	0.62	0.37
4	18.00	18.00	20.25	9.75	0.54	0.59
5	15.00	15.00	17.25	9.00	0.62	0.45
7	27.75	28.50	33.00	14.25	0.28	0.99
9	14.25	15.00	15.00	9.75	0.63	0.34
10	13.50	14.25	18.75	11.25	0.63	0.38
11	39.00	39.75	50.25	30.75	0.00	1.00
12	13.50	13.50	15.75	9.00	0.67	0.36
13	27.75	28.50	33.75	18.75	0.31	0.77
14	18.75	18.75	23.25	13.50	0.53	0.50
15	28.50	30.00	33.75	15.75	0.25	0.97
16	10.50	10.50	12.00	4.50	0.72	0.41
17	15.00	15.00	18.00	9.00	0.63	0.46
18	14.25	15.00	18.75	9.75	0.61	0.46
19	24.00	22.50	26.25	12.75	0.40	0.75
20	22.50	21.75	23.25	14,25	0.44	0.56
22	29.25	31.50	39.75	21.00	0.18	0.96
23	27.00	27.00	30.00	17.25	0.33	0.73
24	14.25	15.00	18.75	11.25	0.63	0.38
25	14.25	14.25	16.50	9.00	0.65	0.40
26	12.00	11.25	14.25	8.25	0.71	0.31
28	13.50	13.50	16.50	8.25	0.66	0.42
29	23.25	22.50	26.25	14.25	0.43	0.65
30	12.00	12.75	14.25	8.25	0.70	0.33
31	20.25	21.00	22.50	14.25	0.49	0.48
32	29.25	30.00	33.75	18.75	0.26	0.83

Table A2.1

Sample HS-1

Meas	# A	В	С	E	Norm	alized
	microns	microns	microns	microns	radius	rate
1	22.50	22.50	29.25	15.00	0.34	1.00
3	15.00	15.00	16.50	5.25	0.55	0.89
5	14.25	14.25	18.00	9.75	0.60	0.58
6	11.25	11.25	13.50	7.50	0.70	0.42
7	11.25	11.25	12.75	6.75	0.69	0.46
8	26.25	26.25	30.75	18.00	0.31	0.92
9	18.75	18.00	21.00	12.00	0.51	0.67
10	21.00	22.50	28.50	14.25	0.35	1.00
11	34.50	34.50	48.00	33.75	0.00	1.00
12	24.00	23.25	30.75	16.50	0.31	1.00
13	21.75	22.50	27.00	13.50	0.39	0.95
14	15.00	15.00	18.75	9.75	0.58	0.63
15	17.25	17.25	19.50	10.50	0.53	0.69
17	26.25	24.75	30.00	15.00	0.30	1.08
18	9.00	9.75	11.25	5.25	0.74	0.42
19	16.50	15.75	21.00	10.50	0.52	0.74
20	13.50	12.75	16.50	9.00	0.63	0.53
21	20.25	19.50	25.50	15.00	0.44	0.74
22	36.75	37.50	47.25	33.00	0.01	1.00
23	12.00	12.00	15.00	8.25	0.67	0.47
24	19.50	19.50	23.25	12.00	0.48	0.79
25	13.50	13.50	15.75	8.25	0.63	0.54
27	15.00	15.00	18.00	9.75	0.60	0.58
28	14.25	14.25	17.25	8.25	0.61	0.63
29	12.75	12.00	14.25	9.00	0.68	0.39
30	15.00	15.00	18.00	9.00	0.59	0.63
32	25.50	26.25	32.25	18.75	0.29	0.95
33	35.25	35.25	44.25	27.75	0.05	1.16
35	24.75	25.50	28.50	20.25	0.36	0.63
36	17.25	17.25	18.00	12.00	0.54	0.51
38	21.75	24.00	29.25	18.75	0.37	0.74

Table A2.1

Sample H-2

Meas	# A	В	С	E	Norm	nalized
	microns	microns	microns	microns	radius	rate
1	7.50	6.75	9.75	6.75	0.80	0.18
2	15.00	15.00	18.00	12.00	0.63	0.36
4	15.00	15.00	14.25	6.00	0.56	0.69
5	15.75	16.50	18.75	11.25	0.59	0.47
6	25.50	22.50	29.25	16.50	0.38	0.77
7	7.50	7.50	9.00	6.00	0.82	0.18
8	36.75	38.25	48.75	32.25	0.00	1.00
9	24.00	23.25	29.25	17.25	0.38	0.73
11	18.75	18.75	24.00	13.50	0.49	0.64
12	18.75	18.75	21.75	12.75	0.52	0.57
13	18.75	18.75	22.50	13.50	0.53	0.55
14	19.50	18.75	21.75	14.25	0.52	0.49
15	29.25	30.00	33.75	18.75	0.22	0.98
16	11.25	11.25	13.50	5.25	0.69	0.50
17	15.00	16.50	20.25	8.25	0.54	0.73
18	17.25	17.25	21.00	9.75	0.53	0.68
19	16.50	17.25	21.75	11.25	0.53	0.64
20	26.25	24.75	30.75	18.75	0.36	0.73
21	14.25	15.00	15.75	9.75	0.62	0.42
22	34.50	35.25	45.75	25.50	0.02	1.23
23	15.00	15.00	14.25	3.75	0.53	0.88
24	23.25	23.25	31.50	16.50	0.32	0.91
25	20.25	22.50	30.00	16.50	0.36	0.82
27	18.00	16.50	22.50	15.00	0.54	0.45
28	22.50	22.50	27.75	12.75	0.38	0.91
30	18.75	18.75	21.75	9.00	0.48	0.81
31	24.75	26.25	30.00	18.00	0.35	0.74
32	13.50	14.25	15.75	8.25	0.63	0.49
34	22.50	22.50	26.25	12.75	0.40	0.85
35	12.75	12.75	15.00	7.50	0.66	0.46
36	21.75	21.75	26.25	12.75	0.42	0.82
37	18.75	18.75	23.25	11.25	0.49	0.73
39	14.25	14.25	15.00	12.00	0.65	0.22
41	20.25	21.00	25.50	12.75	0.44	0.77
42	18.75	18.75	25.50	10.50	0.42	0.91
43	26.25	26.25	33.75	19.50	0.28	0.86
44	21.00	21.75	27.00	13.50	0.41	0.82
46	22.50	22.50	27.75	14.25	0.39	0.82

Table A2.1

Sample H-3

Meas	# A	В	С	E	Norm	alized
	microns	microns	microns	microns	radius	rate
1	24.75	25.50	30.00	15.00	0.25	0.61
2	11.25	11.25	15.00	7.50	0.62	0.30
3	13.50	14.25	15.75	9.00	0.59	0.29
4	15.75	15.00	15.00	7.50	0.50	0.40
6	20.25	20.25	24.00	12.00	0.39	0.49
7	27.75	30.75	37.50	12.75	0.00	1.00
9	18.00	18.75	21.75	12.00	0.46	0.40
10	32.25	33.00	37.50	21.00	0.03	0.71
11	18.75	19.50	21.75	9.00	0.39	0.55
12	33.00	33.00	39.00	21.75	0.03	0.71
13	15.00	15.00	18.00	9.75	0.56	0.33
14	11.25	11.25	14.25	6.75	0.64	0.30
15	23.25	22.50	30.00	15.00	0.25	0.61
16	15.00	14.25	15.75	8.25	0.54	0.35
17	18.00	18.75	22.50	9.00	0.41	0.55
19	24.00	22.50	27.00	12.00	0.28	0.63
20	22.50	21.75	24.75	11.25	0.30	0.60
21	18.75	18.00	22.50	9.00	0.41	0.55
22	15.75	15.75	18.75	9.75	0.53	0.36
23	11.25	11.25	15.00	6.75	0.62	0.33
25	16.50	15.75	19.50	9.75	0.51	0.39
26	14.25	14.25	17.25	9.75	0.58	0.30
27	16.50	16.50	19.50	7.50	0.48	0.49
28	26.25	27.75	30.00	15.00	0.16	0.67
29	15.00	15.75	18.75	10.50	0.54	0.33
30	17.25	16.50	19.50	7.50	0.46	0.51
31	15.00	14.25	15.75	7.50	0.54	0.39
32	9.00	9.00	11.25	6.00	0.72	0.21
33	14.25	15.00	18.00	8.25	0.54	0.39
34	21.00	20.25	25.50	10.50	0.34	0.61
35	9.00	9.00	11.25	4.50	0.71	0.27

## Table A2.1

Sample H-4

Meas	# A	В	С	E	Norm	alized
	microns	microns	microns	microns	radius	rate
1	15.00	15.00	17.25	7.50	0.69	0.33
2	36.00	36.00	43.50	22.50	0.29	0.67
4	12.00	11.25	14.25	6.75	0.76	0.24
5	18.75	19.50	24.75	9.00	0.57	0.50
6	14.25	15.00	17.25	8.25	0.71	0.29
7	10.50	10.50	13.50	6.00	0.77	0.24
8	13.50	13.50	15.75	8.25	0.73	0.25
11	21.75	22.50	26.25	11.25	0.55	0.48
12	15.00	15.00	16.50	7.50	0.69	0.32
13	9.75	9.75	12.00	5.25	0.80	0.21
14	13.50	13.50	16.50	6.00	0.71	0.33
15	13.50	13.50	15.75	9.00	0.74	0.22
16	10.50	10.50	14.25	7.50	0.77	0.21
17	21.75	22.50	27.00	12.00	0.54	0.48
18	12.00	12.00	15.75	8.25	0.74	0.24
20	21.00	22.50	27.00	14.25	0.56	0.40
22	15.00	15.00	17.25	6.75	0.69	0.35
23	48.75	45.00	60.00	28.50	0.00	1.00
24	33.75	36.00	44.25	18.75	0.25	0.81
25	15.75	15.00	18.75	9.00	0.69	0.31
27	10.50	11.25	13.50	6.75	0.78	0.21
29	22.50	21.00	26.25	7.50	0.53	0.60
30	8.25	8.25	9.00	3.00	0.82	0.22
31	23.25	24.00	27.00	10.50	0.50	0.56
33	11.25	12.00	14.25	7.50	0.77	0.21
34	8.25	8.25	11.25	5.25	0.81	0.19
37	15.00	15.00	18.75	7.50	0.68	0.36
38	9.00	9.00	10.50	5.25	0.82	0.17
39	16.50	17.25	18.75	11.25	0.67	0.26
40	23.25	22.50	30.00	12.75	0.49	0.55

Table A2.1

Sample SC34D

Meas	# A	В	С	E	Norm	alized
	microns	microns	microns	microns	radius	rate
				<del></del>		<del> </del>
1	15.75	15.75	16.88	9.00	0.65	0.32
2	21.38	21.38	22.50	11.25	0.52	0.46
3	29.25	29.25	34.88	18.00	0.38	0.58
4	25.88	25.88	29.25	13.50	0.43	0.59
5	30.38	30.38	34.88	15.75	0.33	0.69
6	22.50	22.50	28.13	13.50	0.50	0.50
7	20.25	20.25	23.63	9.00	0.55	0.52
8	21.38	21.38	24.75	10.13	0.52	0.52
9	23.63	23.63	28.13	13.50	0.50	0.50
10	21.38	21.38	23.63	10.13	0.52	0.52
11	22.50	22.50	22.50	7.88	0.46	0.64
12	21.38	21.38	27.00	12.38	0.51	0.50
13	45.00	45.00	49.50	23.63	0.00	1.00
14	21.38	21.38	24.75	12.38	0.54	0.44
15	11.25	11.25	12.38	3.38	0.73	0.35
16	30.38	30.38	34.88	18.00	0.35	0.61
17	21.38	21.38	22.50	9.00	0.50	0.56
18	16.88	16.88	19.13	12.38	0.65	0.25
19	18.00	18.00	21.38	6.75	0.59	0.50
20	12.38	12.38	15.75	5.63	0.70	0.35
22	27.00	27.00	28.13	13.50	0.39	0.61

Table A2.1

Sample SC34E

Meas	# A	В	C	E	Norm	alized
	microns	microns	microns	microns	radius	rate
1	53.25	54.75	74.25	42.00	0.09	0.89
5	28.50	30.00	33.75	11.25	0.52	0.66
8	26.25	26.25	30.00	13.50	0.59	0.49
9	42.75	41.25	52.50	30.00	0.36	0.62
10	45.00	44.25	53.25	28.50	0.34	0.69
12	33.75	33.75	37.50	19.50	0.48	0.56
13	33.00	33.75	34.50	18.00	0.47	0.56
15	29.25	28.50	34.50	15.00	0.55	0.54
17	15.00	15.00	18.75	8.25	0.76	0.29
18	65.25	63.00	67.50	37.50	0.00	1.00
19	33.00	33.00	36.75	12.75	0.45	0.74
21	24.00	24.00	27.00	15.75	0.64	0.34
22	56.25	60.00	65.25	34.50	0.11	0.94
28	36.00	33.75	45.75	24.75	0.43	0.58
29	30.75	30.00	36.75	15.00	0.52	0.60
30	36.00	36.75	45.00	24.00	0.44	0.58
31	63.75	62.25	76.50	43.50	0.06	0.92
32	27.75	30.00	35.25	21.75	0.58	0.37
34	29.25	30.75	36.00	15.00	0.53	0.58
35	25.50	26.25	30.75	9.00	0.58	0.61
38	48.00	48.75	58.50	27.75	0.25	0.85
40	18.75	18.75	21.00	6.75	0.69	0.43

Table A2.1

Sample SC39D

Meas	# A	В	С	E	Norm	alized
	microns	microns	microns	microns	radius	rate
2	14.25	13.50	15.00	8.25	0.75	0.38
3	18.75	19.50	24.00	15.75	0.67	0.40
4	30.00	30.00	38.25	22.50	0.45	0.77
5	33.00	34.50	41.25	26.25	0.42	0.73
6	26.25	25.50	30.75	18.00	0.56	0.62
7	43.50	44.25	52.50	34.50	0.27	0.88
8	13.50	13.50	15.00	7.50	0.75	0.41
10	48.75	48.75	52.50	36.75	0.17	0.89
11	41.25	42.75	48.75	34.50	0.31	0.72
12	33.75	34.50	43.50	29.25	0.40	0.69
13	21.00	21.00	24.00	15.00	0.64	0.47
14	30.00	28.50	37.50	22.50	0.47	0.73
15	60.00	62.25	70.50	51.00	0.00	1.00
16	31.50	33.75	41.25	23.25	0.41	0.88
17	33.75	33.75	39.00	20.25	0.40	0.96
18	33.75	33.75	37.50	22.50	0.41	0.81
20	50.25	48.75	63.75	36.75	0.09	1.31
23	24.75	26.25	30.75	22.50	0.59	0.40
24	12.75	13.50	17.25	9.00	0.75	0.40
25	33.00	33.75	39.75	25.50	0.44	0.70
26	22.50	24.00	29.25	18.75	0.59	0.51

Table A2.1

Sample Sal-8

Meas	# A	В	C	E	Norm	alized
	microns	microns	microns	microns	radius	rate
1	12.00	10.50	13.50	8.25	0.61	0.86
2	25.50	26.25	28.50	24.00	0.16	0.83
3	20.25	20.25	22.50	19.50	0.35	0.54
4	13.50	13.50	16.50	12.75	0.56	0.61
5	32.25	31.50	37.50	31.50	0.00	1.00
6	22.50	22.50	28.50	24.00	0.26	0.73
7	11.25	11.25	13.50	12.00	0.66	0.24
8	28.50	29.25	30.75	23.25	0.01	1.45
9	26.25	27.75	31.50	22.50	0.10	1.52
11	19.50	20.25	20.25	17.25	0.34	0.61
12	13.50	14.25	17.25	15.75	0.57	0.24
13	27.75	27.75	31.50	24.75	0.09	1.19
14	8.25	8.25	10.50	9.00	0.73	0.24
15	23.25	24.00	28.50	24.75	0.27	0.61
16	26.25	27.75	36.00	30.75	0.07	0.86
17	9.00	9.00	10.50	8.25	0.71	0.38
18	15.00	15.00	18.75	15.00	0.50	0.61
19	11.25	12.00	15.00	13.50	0.62	0.24
21	23.25	24.00	26.25	22.50	0.24	0.68

Table A2.1 (cont)

Sample Sal-5

Meas	# A	В	С	C E		nalized
	microns	microns	microns	microns	radius	rate
1	33.75	36.75	43.50	37.50	0.07	0.85
2	13.50	13.50	15.00	12.75	0.64	0.35
3	15.75	16.50	21.00	17.25	0.54	0.53
4	18.00	18.00	16.50	15.00	0.50	0.31
6	24.00	24.75	28.50	24.75	0.37	0.55
7	13.50	14.25	15.75	12.75	0.63	0.46
8	15.00	14.25	16.50	14.25	0.62	0.35
10	37.50	39.00	44.25	37.50	0.00	1.00
13	13.50	14.25	15.00	13.50	0.63	0.25
14	26.25	26.25	28.50	24.75	0.30	0.61
16	26.25	26.25	30.75	26.25	0.32	0.65
17	17.25	18.00	21.75	18.75	0.53	0.42
19	25.50	24.00	30.00	25.50	0.35	0.64
21	15.00	15.75	19.50	15.00	0.56	0.64
22	22.50	24.00	26.25	22.50	0.39	0.58
23	15.75	15.00	18.75	15.75	0.59	0.42
24	27.75	26.25	31.50	27.75	0.31	0.55
25	11.25	11.25	14.25	12.00	0.69	0.32
26	27.75	28.50	30.75	26.25	0.25	0.72
27	28.50	29.25	34.50	31.50	0.28	0.42
28	20.25	19.50	22.50	18.00	0.46	0.69
30	31.50	33.75	39.00	33.00	0.16	0.85

Table A2.1

Sample M-9

Meas	# A	В	С	E	Norm	nalized
	microns	microns	microns	microns	radius	rate
1	29.25	29.25	34.88	20.25	0.29	0.70
2	24.75	24.75	30.38	21.38	0.41	0.43
3	34.88	34.88	45.00	28.13	0.10	0.80
4	15.00	15.00	15.00	12.00	0.64	0.18
5	15.00	15.00	15.75	9.75	0.62	0.34
6	18.75	18.75	21.75	12.75	0.54	0.45
7	22.50	22.50	24.00	13.50	0.42	0.59
8	27.00	27.00	30.75	16.50	0.31	0.73
9	16.50	16.50	18.00	8.25	0.56	0.53
10	39.00	39.00	48.75	27.75	0.00	1.00
11	15.75	15.75	18.75	11.25	0.62	0.36
12	21.00	21.00	25.50	13.50	0.47	0.57
13	16.50	16.50	18.00	8.25	0.56	0.53
14	16.50	16.50	18.75	11.25	0.59	0.38
15	10.50	10.50	11.25	5.25	0.72	0.33
16	13.50	13.50	15.75	10.50	0.68	0.26
17	25.50	25.50	31.50	18.00	0.35	0.64
18	23.25	23.25	24.75	15.00	0.41	0.55
19	10.50	10.50	12.00	5.25	0.72	0.34
20	38.25	38.25	44.25	26.25	0.06	0.90
21	32.25	32.25	38.25	24.00	0.23	0.68
22	27.75	27.75	32.25	21.75	0.34	0.52
23	33.75	33.75	41.25	21.75	0.14	0.93
24	6.00	6.00	7.50	4.50	0.85	0.14
25	9.75	9.75	11.25	6.75	0.76	0.23
26	27.00	27.00	31.50	15.00	0.31	0.81
27	13.50	13.50	15.75	9.75	0.67	0.30
28	14.25	14.25	17.25	0.75	0.57	0.79
29	24.75	24.75	30.00	20.25	0.41	0.46
30	37.50	37.50	46.50	30.00	0.08	0.79
31	36.00	36.00	41.25	32.25	0.18	0.46
32	27.00	27.00	32.25	18.00	0.34	0.68
33	9.75	9.75	12.75	6.00	0.73	0.32
34	13.50	13.50	14.25	5.25	0.62	0.51
35 36	15.00	15.00	16.50	12.75	0.65	0.20
36	28.50	28.50	33.00	22.50	0.32	0.52
37	18.75	18.75	22.50	14.25	0.55	0.39
38	20.25	20.25	<b>21.75</b> .	15.75	0.51	0.33

Table A2.1

Sample J1V

Meas	# A	В	С	E	Norm	nalized
	microns	microns	microns	microns	radius	rate
2	25.50	25.50	29.25	18.00	0.34	0.88
5	22.50	22.50	26.25	18.75	0.45	0.58
6	26.25	27.75	28.50	20.25	0.31	0.73
7	18.75	19.50	22.50	12.75	0.50	0.74
8	15.00	15.00	17.25	9.75	0.61	0.59
9	21.00	21.00	27.75	16.50	0.41	0.83
10	30.00	30.75	32.25	24.00	0.23	0.73
12	18.00	18.75	20.25	13.50	0.53	0.56
13	17.25	18.00	21.00	15.00	0.57	0.45
15	12.38	12.38	15.75	6.75	0.64	0.67
16	25.50	26.25	33.00	18.75	0.29	1.06
18	21.38	20.25	24.19	15.75	0.47	0.65
19	24.75	24.00	29.25	19.50	0.39	0.72
20	24.00	24.75	30.75	18.75	0.35	0.89
21	38.25	39.38	49.50	36.00	0.00	1.00
23	24.75	24.75	28.13	16.88	0.35	0.90
24	21.38	22.50	24.75	18.00	0.46	0.54
25	25.88	25.88	33.75	21.38	0.29	0.92
26	21.38	22.50	25.88	15.75	0.44	0.76
27	11.25	11.25	13.50	5.63	0.69	0.58
28	12.38	12.38	14.63	7.88	0.68	0.51
29	15.75	14.63	19.13	9.00	0.57	0.75
30	18.00	16.88	20.25	13.50	0.56	0.52
31	36.00	34.88	45.00	33.75	0.10	0.83
32	15.00	15.00	18.75	12.00	0.61	0.50
33	26.25	25.50	32.25	24.00	0.35	0.61

Table A2.1

Sample J-1

Meas	# A	A B C		E	Norm	alized
	microns	microns	microns	microns	radius	rate
2	32.25	30.75	39.00	32.25	0.39	0.47
4	35.25	36.00	45.00	39.75	0.31	0.37
5	30.00	29.25	34.50	30.00	0.45	0.33
6	21.00	23.25	27.00	21.00	0.57	0.42
7	25.50	25.50	29.25	23.25	0.51	0.44
8	15.75	16.50	19.50	18.00	0.71	0.10
9	18.75	19.50	26.25	21.75	0.59	0.31
11	20.25	20.25	26.25	21.75	0.59	0.31
14	51.00	51.00	58.50	45.00	0.00	1.00
15	22.50	21.75	19.50	10.50	0.48	0.95
16	32.25	31.50	31.50	18.00	0.28	1.23
18	24.00	24.00	23.25	12.00	0.44	1.05
19	36.00	37.50	38.25	26.25	0.22	1.02
21	35.25	35.25	33.00	26.25	0.26	0.66
23	15.00	15.75	18.75	15.75	0.71	0.21
24	34.50	32.25	42.00	36.00	0.35	0.42
25	16.88	16.88	16.88	7.88	0.60	0.81
26	31.50	31.50	33.75	24.75	0.35	0.74
27	18.00	18.00	21.38	12.38	0.62	0.63
28	15.75	15.75	21.38	12.38	0.63	0.63
29	21.38	21.38	23.63	14.06	0.54	0.75
30	22.50	22.50	23.63	14.63	0.51	0.76
32	20.25	20.25	22.50	12.38	0.56	0.79
33	22.50	23.63	27.00	15.75	0.51	0.81
34	25.88	24.75	33.75	21.38	0.42	0.86
36	28.13	28.13	31.50	14.63	0.37	1.29
37	21.38	21.38	22.50	11.25	0.51	0.94
38	15.75	14.63	19.13	11.25	0.67	0.55
39	24.75	27.00	33.75	19.13	0.41	1.02
41	33.75	33.75	39.38	28.13	0.33	0.81

Table A2.1

Sample J1H

Meas	# A	В	C E	Normalized		
	microns	microns	microns	microns	radius	rate
2	32.25	30.75	39.00	32.25	0.39	0.47
4	35.25	36.00	45.00	39.75	0.31	0.37
5	30.00	29.25	34.50	30.00	0.45	0.33
6	21.00	23.25	27.00	21.00	0.57	0.42
7	25.50	25.50	29.25	23.25	0.51	0.44
8	15.75	16.50	19.50	18.00	0.71	0.10
9	18.75	19.50	26.25	21.75	0.59	0.31
11	20.25	20.25	26.25	21.75	0.59	0.31
14	51.00	51.00	58.50	45.00	0.00	1.00
15	22.50	21.75	19.50	10.50	0.48	0.95
16	32.25	31.50	31.50	18.00	0.28	1.23
18	24.00	24.00	23.25	12.00	0.44	1.05
19	36.00	37.50	38.25	26.25	0.22	1.02
21	35.25	35.25	33.00	26.25	0.26	0.66
23	15.00	15.75	18.75	15.75	0.71	0.21
24	34.50	32.25	42.00	36.00	0.35	0.42

# APPENDIX III

#### Appendix 3

The Mg concentrations from Patterson and Kinsman (1982) were recalculated to reflect the excess of Mg<sup>2+</sup> in solution relative to equilibrium with dolomite in an aragonite buffered system. This was found by assuming that dolomite precipitation follows:

A3.1 
$$CaMg(CO_3)_2 \iff Ca^{2+} + Mg^{2+} + 2CO_3^{2-}$$

The equilibrium condition for this reaction is therefore:

A3.2 
$$K_{Dol} = [Ca^{2+}] [Mg^{2+}] [CO_3^{2-}]^2$$

Assuming that the system is buffered by aragonite requires that for the reaction:

A3.3 
$$CaCO_3 \iff Ca^{2+} + CO_3^{2-}$$

the equilibrium condition is :

A3.4 
$$K_{Arag} = [Ca^{2+}][CO_3^{2-}]$$

Rearranging A3.4 and substituting into A3.2 provides an expression for the equilibrium  $[Mg^{2+}]$  when given the  $[Ca^{2+}]$ 

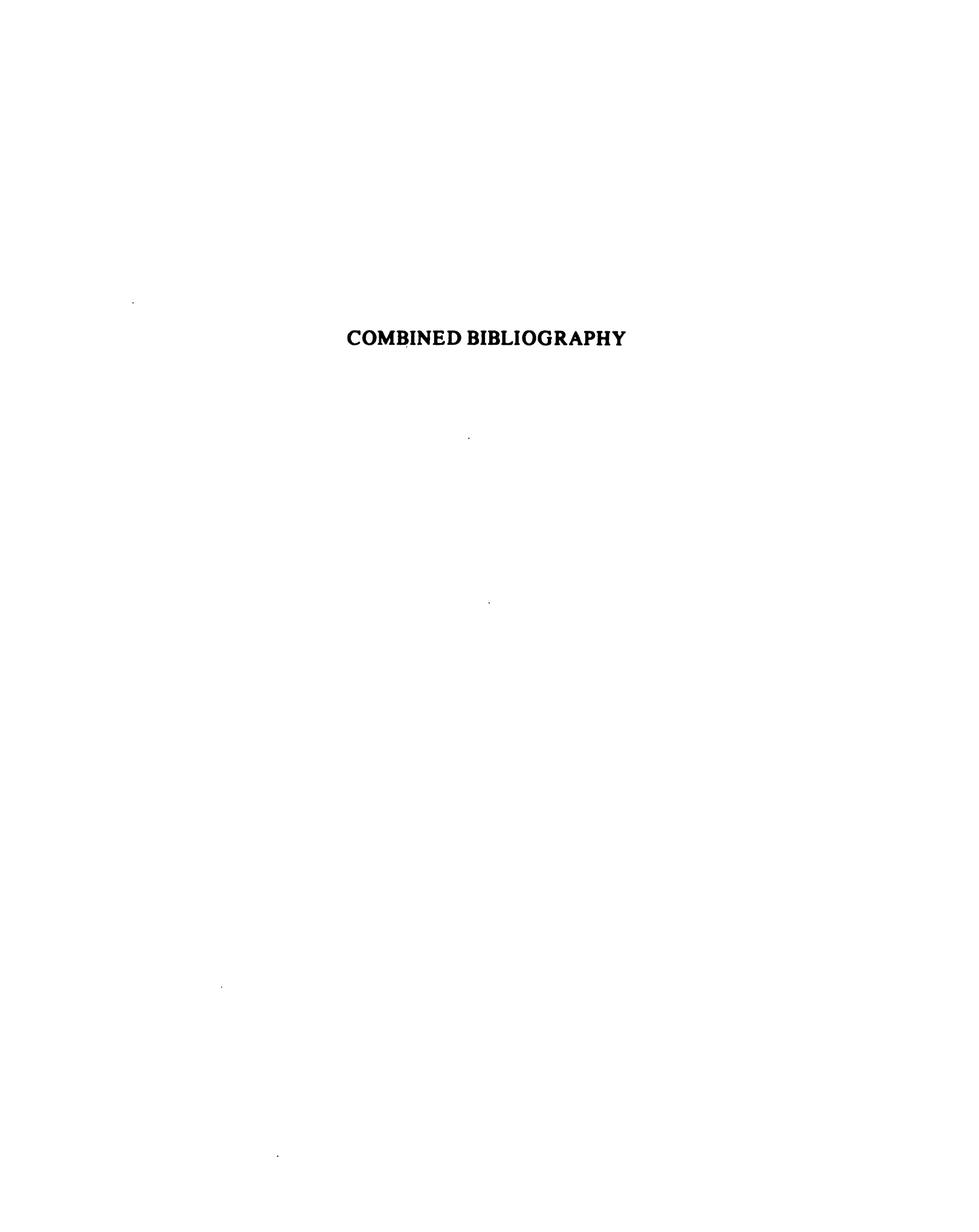
during precipitation of dolomite in an aragonite buffered system.

A3.5 
$$[Mg^{2+}] = [Ca^{2+}] K_{Dol}/K_{Arag}^2$$

Table A3

 ${\rm Mg^{2+}}$  concentration in excess of dolomite equilibrium in an aragonite buffered system. Original data from Patterson and Kinsman (1982) was modified using A3.5 and assuming a  ${\rm K_{DOl}}$  of  ${\rm 10^{-17}}$  and a  ${\rm K_{Arag}}$  of  ${\rm 10^{-8\cdot37}}$ 

mCa <sup>2+</sup>	mMg <sup>2+</sup>	Depth (cm)	mMg <sup>2+</sup> eq	Mg-Mg <sub>eq</sub>	Depth	c(x)
100 Kg	100 Kg	(Cm)	100 Kg	100 Kg	(m)	co
	· · · · · · · · · · · · · · · · · · ·	L	ocation Ca	A' 1		
1.63	33.6	22	2.71	30.88	0.0	1.00
1.76	31.9	24	2.93	28.97	0.02	0.94
1.87	31.6	24	3.11	28.48	0.02	0.92
1.88	30.9	49	3.13	27.77	0.27	0.90
2.11	31.1	78	3.51	27.59	0.56	0.89
2.31	29.2	100	3.84	25.35	0.78	0.82
		L	ocation C	C'4		
2.17	29.2	15	3.61	25.59	0.0	1.00
2.34	28.5	31	3.89	24.10	0.16	0.94
2.70	26.5	57	4.49	22.00	0.42	0.86
2.88	26.5	79	4.79	21.71	0.64	0.85
<del> </del>		L	ocation C	C'1		<del></del>
3.00	24.9	15	4.99	19.91	0.0	1.00
3.38	23.3	31	5.62	17.67	0.16	0.89
3.88	21.2	50	6.45	14.74	0.39	0.74
4.18	20.9	79	6.95	13.94	0.64	0.70
4.30	20.5	98	7.15	13.34	0.83	0.67



- Baker, P.A. and Burns, S.J., 1985, Occurrence and Formation of Dolomite in Organic-Rich Continental Margin Sediments, The American Association of Petroleum Geologists Bulletin, v 69, p 1917-1930.
- Baker, P.A. and Kastner, M., 1981, Constraints on the formation of sedimentary dolomite, Science, v. 213, p. 214-216.
- Banner, J.L., Hanson, G.N. and Meyers, W.J., 1988, Water-Rock Interaction History of Regionally Extensive Dolomites of the Burlington-Keokuk Formation (Mississippian): Isotopic Evidence, in Shukla and Baker (ed.) Sedimentology and Geochemistry of Dolostones, SEPM Special Publication No. 43, p. 97-113.
- Banner, J.L., Hanson, G.N. and Meyers, W.J., 1988a,
  Determination of initial Sr isotopic compositions of
  dolostones from the Burlington-Keokuk formation
  (Mississippian): Constraints from cathodoluminescence,
  glauconite paragenesis and analytical methods. Jour.
  Sed. Petrology, V 58, p 673-687.
- BeMent, W.O., Elias, R.J., Goodman, W.R., Bacon, R., Yu, H.S., Potter, P.E., 1981, Mississippian and Pennsylvanian section on Interstate 75 south of Jellico, Campbell County, Tennessee, Report of Investigations, Division of Geology, V 38, 42p.
- Berner, R.A., 1971, Principles of Chemical Sedimentology, McGraw-Hill, New York, 240 p.
- Berner, R.A., 1980, Early Diagenesis; A Theoretical Approach, Princeton University Press, Princeton, N.J. 241 p.
- Brown, C.D. jr., and L.A. Lineback, 1966, Lithostratigraphy of Cincinnatian Series (Upper Ordovician) in Southwestern Indiana. A.A.P.G., V. 50, p 1018-1032.
- Burton, W.K., Cabrera, N. and Frank, F.C., 1951, The growth of crystals and the equilibrium structure of their surfaces, Phil. Trans. Royal Soc. London, A234, p 299-358.
- Butler, G., 1969, Modern evaporite deposition and geochemistry of coexisting brines, the Sabkha, Trucial Coast, Arabian Gulf, Journal of Sedimentary Petrology, V. 39, p. 70-89.

- Cander, H.S., Kaufman, J., Daniels, L.D., and Meyers, W.J., 1988, Regional Dolomitization of Shelf Carbonates in the Burlington-Keokuk (Mississippian), Illinois and Missouri: Constraints from Cathodoluminescent Zonal Stratigraphy, in Shukla and Baker (ed.), Sedimentology and Geochemistry of Dolostones, SEPM Special Publication No. 43, p. 129-144.
- Carlson, M.P. 1979, The Nebraska-Iowa Region, in Craig, L.C. and Varnes, K.L., eds., Paleotectonic Investigations of the Mississippian System in the United States, Part I: Introduction and Analyses of the Mississippian System: U.S. Geological Survey Professional Paper No 1010-F, p 107-114.
- Carlson, W.D., 1989, The significance of intergranular diffusion to the mechanisms and kinetics of porphyroblast crystallization., Contributions to Mineralogy and Petrology, V 103, p. 1-24.
- Carpenter A.B. 1980, The chemistry of dolomite formation 1: The stability of dolomite. In Concepts and models of dolomitization (ed. D.H. Zenger et al.): SEPM Spec. Publ. 28, 111-121.
- Choquette, P.W., Cox, A., Meyers, W.J., 1991, Characteristics, distribution and origin of porosity in shelf dolostones: Burlington-Keokuk Formation (Mississippian), U.S. mid-continent.
- Chowns, T.M., Elkins, J.E., 1974, The origin of quartz geodes and cauliflower cherts through the silicification of anhydrite nodules, Journal of Sedimentary Petrology, V 44, p 885-903.
- Compton, J.S., 1988, Degree of supersaturation and precipitation of organogenic dolomite, Geology, v 16, p 318-321.
- De Buisonje, P.H., 1974, Neogene and Quaternary Geology of Aruba, Curacao and Bonaire, Martinus Nijhoff, The Hague 291 p.
- Dunning W.J., 1969, General and theoretical introduction. in *Nucleation* (ed. A.C. Zettlemoyer): Marcel Dekker, Inc. 1-67.
- Fouke, B.W., Reeder, R.J., 1992, Surface structural controls on dolomite composition, evidence from sector zoning, Geochim et Cosmochim. Act., V 56, p 4015-4024.
- Freeze, R.A., Cherry, J.A., Groundwater, Prentice-Hall, Englewood Cliffs, New Jersey, 604 p.

- Fuchtbauer H., and Goldschmidt H., 1965, Beziehungen zwischen calciumgehalt und bilungsbedingungen der dolomite. Geol. Rundsch., 55, 84-101.
- Gaines A., 1980, Dolomitization kinetics. In Concepts and models of dolomitization (ed. D.H. Zenger et al.): SEPM Spec. Publ. 28, 123-137.
- Goldsmith J.R., Graf D.L., 1958, Structural and compositional variations in some natural dolomites. *J. Geol.* 66, 678-693.
- Goldsmith J.R., Graf D.L., and Heard H.C., 1961, Lattice constants of the calcium-magnesium carbonates. Amer. Mineral., 46, 453-457.
- Hardie L.A. ,1987, Dolomitization. A critical view of some current views. Jour. Sed. Petrol., 57, 166-183.
- Hatfield, C.B., 1968, Stratigraphy and Paleoecology of the Saluda Formation (Cincinnatian) in Indiana, Ohio Kentucky., G.S.A. Special Paper 95.
- Katz A. and Matthews A., 1977, The dolomitization of CaCO<sub>3</sub>: An experimental study at 252-295° C. Geochim. Cosmochim. Acta, 41, 297-308.
- Kaufman, J., Cander, H.S., Daniels, L.D., Meyers, W.J., 1988, Calcite cement stratigraphy and cementation history of the Burlington-Keokuk Formation (Mississippian), Illinois and Missouri. Jour. Sed. Petrology, V 58, p 312-326.
- Kretz, R., 1974, Some models for the rate of crystallization of garnet in metamorphic rocks., Lithos, Vol. 7, p. 123-131.
- Lucia, F.J., Major R.P., in prep
- Lumsden D.N., and Chimahusky J.S., 1980, The Relationship between dolomite nonstoichiometry and carbonate facies parameters, In Concepts and models of dolomitization (ed. D.H. Zenger et al.): SEPM Spec. Publ. 28, 123-137.
- Machel H.G. and Mountjoy E.W., 1986, Chemistry and environments of dolomitization A reappraisal. Earth Science Rev, 23, 175-222.
- Machel, H.G. and Mountjoy, E.W., 1986, Chemistry and Environments of Dolomitization - A Reappraisal, Earth-Science Reviews, V 23, p 175-222.

- Martin, W.D., 1975, Petrology of Cincinattian Series Limestones. Journal of Sedimentary Petrology, V.45, p. 907-925.
- Mazzulo, S.J., Reid, A.M., Gregg, J.M., 1987, Dolomitization of Holocene Mg-calcite supratidal deposits, Ambergris Cay, Belize, Geological Society of America, v 98, p 224-231.
- Middelburg, J.J., de Lange, G.j., Kreulen, R., 1990, Dolomite formation in anoxic sediments of Kau Bay, Indonesia, Geology, v 18, p. 399-402.
- Morse J.W., and Casey W.H., 1988, Ostwald processes and mineral paragenesis in sediments. Am. Jour. Sci., 288, 537-560.
- Morse, J.W., 1983, The Kinetics of calcium carbonate dissolution and precipitation, in Reeder R.J. (ed.), Carbonates: Mineralogy and Chemistry, Mineralogical Society of America, p 277-264.
- Mucci A., 1986, Growth kinetics and composition of magnesium calcite overgrowths precipitated from seawater: quantitative influence of orthophosphate ions, Geochim et Cosmochim Acta, V 50, p 2255-2265.
- Mucci A., Canuel, R., Zhong, S., 1989, The solubility of calcite and aragonite in sulfate-free seawater and the seeded growth kinetics and composition of the precipitates at 25°C, Chemical Geology, V 74, p 309-320.
- Mucci A., Morse, J.W., 1983, The incorporation of  $Mg^{2+}$  and  $Sr^{2+}$  into calcite overgrowths: influences of growth rate and solution composition, Geochim et Cosmochim, V 47, p 217-233.
- Nielsen, A.E., 1964, Kinetics of precipitation, Macmillan, New York, 151 p.
- Ohara, M, Reid, R.C., 1973, Modeling Crystal Growth Rates from Solution, Prentice-Hall, Englewood cliffs, N.J., 272 p.
- Palciauskas, V.V., Domenico, P.A., 1976, Solution chemistry, mass transfer, and the approach to chemical equilibrium in porous carbonate rocks. Geol. Soc. of Amer. Bull., V 87, p 207-214.

- Martin, W.D., 1975, Petrology of Cincinattian Series Limestones. Journal of Sedimentary Petrology, V.45, p. 907-925.
- Mazzulo, S.J., Reid, A.M., Gregg, J.M., 1987, Dolomitization of Holocene Mg-calcite supratidal deposits, Ambergris Cay, Belize, Geological Society of America, v 98, p 224-231.
- Middelburg, J.J., de Lange, G.j., Kreulen, R., 1990, Dolomite formation in anoxic sediments of Kau Bay, Indonesia, Geology, v 18, p. 399-402.
- Morse J.W., and Casey W.H., 1988, Ostwald processes and mineral paragenesis in sediments. Am. Jour. Sci., 288, 537-560.
- Morse, J.W., 1983, The Kinetics of calcium carbonate dissolution and precipitation, in Reeder R.J. (ed.), Carbonates: Mineralogy and Chemistry, Mineralogical Society of America, p 277-264.
- Mucci A., 1986, Growth kinetics and composition of magnesium calcite overgrowths precipitated from seawater: quantitative influence of orthophosphate ions, Geochim et Cosmochim Acta, V 50, p 2255-2265.
- Mucci A., Canuel, R., Zhong, S., 1989, The solubility of calcite and aragonite in sulfate-free seawater and the seeded growth kinetics and composition of the precipitates at 25°C, Chemical Geology, V 74, p 309-320.
- Mucci A., Morse, J.W., 1983, The incorporation of  $Mg^{2+}$  and  $Sr^{2+}$  into calcite overgrowths: influences of growth rate and solution composition, Geochim et Cosmochim, V 47, p 217-233.
- Nielsen, A.E., 1964, Kinetics of precipitation, Macmillan, New York, 151 p.
- Ohara, M, Reid, R.C., 1973, Modeling Crystal Growth Rates from Solution, Prentice-Hall, Englewood cliffs, N.J., 272 p.
- Palciauskas, V.V., Domenico, P.A., 1976, Solution chemistry, mass transfer, and the approach to chemical equilibrium in porous carbonate rocks. Geol. Soc. of Amer. Bull., V 87, p 207-214.

- Patterson, R.J., Kinsman, D.J.J., 1982, Formation of diagenetic dolomite in coastal sabka along Arabian (Persian) Gulf. A.A.P.G. V66, p 28-43.
- Phillips, O.M. 1991, Flow and Reactions in Permeable Rocks, Cambridge University Press, Cambridge, U.K., 285 p.
- Pierre, C., Ortlieb, L., Person, A., 1984, Supratidal Evaporitic Dolomite at Ojo De Liebre Lagoon: Mineralogical and Isotopic Arguments for Primary Crystallization, Journal of Sedimentary Petrology, V. 54, p. 1049-1061.
- Pingatore, N.E. jr., 1976, Vadose and Phreatic Diagenesis: Processes Products and Their Recognition in Coral, Journal Sedimentary Petrology, v 46 p 985-1006.
- Reeder, R.J., Prosky, J.L., 1986, Compositional sector zoning in dolomite, Jour. Sed. Petrology, V 56, p 237-247.
- Royce C.R. Jr., Wadell J.S., and Peterson, L.E., 1971, X-ray determination of calcite-dolomite: An evaluation. Jour. Sed. Petrol., 41, 483-488.
- Sibley, D.F. and Bartlett T.R., 1987, Nucleation as a rate limiting step in dolomitization, in Proceedings, International Symposium on Crystal Growth Processes in the Sedimentary Environment, 2nd, Granada, 1986.

  Madrid, Instituto de Geologica, C.S.I.C., 733-741.
- Sibley, D.F., 1980, Climatic Control of Dolomitization, Seroe Domi Formation (Pliocene), Bonaire, N.A., in Zenger, Dunham and Ethington (ed.), Concepts and Models of Dolomitization, SEPM Special Pub. No. 28, p. 247-258.
- Sibley, D.F., 1990, Unstable to stable transformation during dolomitization. J. Geol., 98, 743-748.
- Sibley, Dedoes R.E., and Bartlett T.R., 1987, Kinetics of dolomitization. Geology, 15, 1112-1114.

MICHIGAN STATE UNIV. LIBRARIES
31293010219586